Department of Physics and Astronomy
University of Heidelberg

Bachelor Thesis in Physics
submitted by

Jonathan Brandt

born in Hanau (Germany)

2018

Development of an Event Display for the Cbm-ToF Cosmic test stand

This Bachelor Thesis has been carried out by Jonathan Brandt at the
Physikalisches Institut at the University of Heidelberg
under the supervision of
Prof. Dr. Norbert Herrmann

Abstract

The future Compressed Baryonic Matter (CBM) experiment includes a Time-of-flight (ToF) wall consisting of Multi-gap Resistive Plate Chambers (MRPCs). In order to test prototypes a test stand measuring cosmic muons has been established in Heidelberg. Within the scope ot this thesis an event display was developed which allows a visual representation of the particles measured with the detectors. This event display was programmed to represent physics observables of the measured hits and to display additional parameters associated with reconstructed particle trajectories. To demonstrate the benefit of an event display as a quality assurance tool several applications have been studied. With the help of the display it was analyzed how the detector and analysis software respond to specific instances and events.

Zusammenfassung

Das zukünftige Compressed Baryonic Matter (CBM) Experiment wird eine Wand zur Flugzeitmessung beinhalten, welche aus Mehrfachspalt-Widerstandsplattenkammern (MRPCs) besteht. Um Prototypen zu testen, wurde in Heidelberg ein Teststand aufgebaut, in welchem Myonen aus der kosmischen Höhenstrahlung detektiert werden. In dieser Arbeit wurde ein Event Display entwickelt, welches eine visuelle Darstellung der detektierten Teilchen ermöglicht. Die programmierten Funktionalitäten beinhalten die Darstellung von physikalischen Observablen, die einem gemessenen Hit zugeordnet sind, sowie weiterer Parameter, die bei der Spur-Rekonstruktion der Teilchenbahnen entstehen. Es wurden mehrere Anwendungen untersucht, um den Nutzen dieses Event Displays in der Qualitätsüberprüfung zu demonstrieren. Dafür wurde das Verhalten von Detektoren und Analyse-Software in einzelnen Events untersucht.

Contents

1 Introduction

1.1 CBM experiment

The Compressed Baryonic Matter experiment (CBM) at the Facility for Antiproton and Ion Research (FAIR) at the Gesellschaft für Schwerionenforschung mbH (GSI) in Darmstadt, Germany is a future heavy-ion fixed-target experiment which aims to explore the phase diagram of strongly interacting matter.

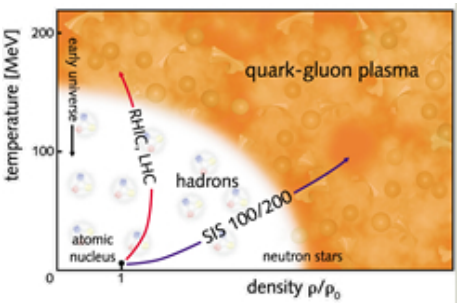

Figure 1.1: Phase diagram of strongly interacting matter as predicted by theory. Sketched are the research regions to which the different accelerators are aiming. Historic, since plans for SIS200 are rejected. Source: [FAI]

CBM aims for the research region of high baryon densities instead of highest temperatures. The latter conditions are explored by other experiments like A Large Ion Collider Experiment (ALICE) at the Large Hadron Collider (LHC) of the European Organization for Nuclear Research (CERN) in Geneva, Switzerland or the Solenoidal Tracker (STAR) detector at the Relativistic Heavy Ion Collider (RHIC) at Brookhaven National Laboratory (BNL) in Upton, United States (see fig. 1.1).

In particular the research program will include the search for phase transitions and exotic forms of strongly interacting matter. The equation-of-state of nuclear matter at densities supposed to prevail in the cores of neutron stars will be studied. The experimental specifications are designed for gold on gold nuclei-collision reaching energies up to 11 AGeV. This will be provided by the SIS100 synchrotron currently under construction at FAIR. Former plans for a SIS200

have been rejected many years ago. A later upgrade to a SIS300 accelerator is still under discussion. The detector is supposed to measure the collective behavior of all particles forming in the collision process. This will happen at interaction rates up to 10 MHz. Therefore CBM is designed with free-streaming data-acquisition and online tracking and particle identification.
The CBM detector consists of several sub-detector systems (fig. 1.2). The

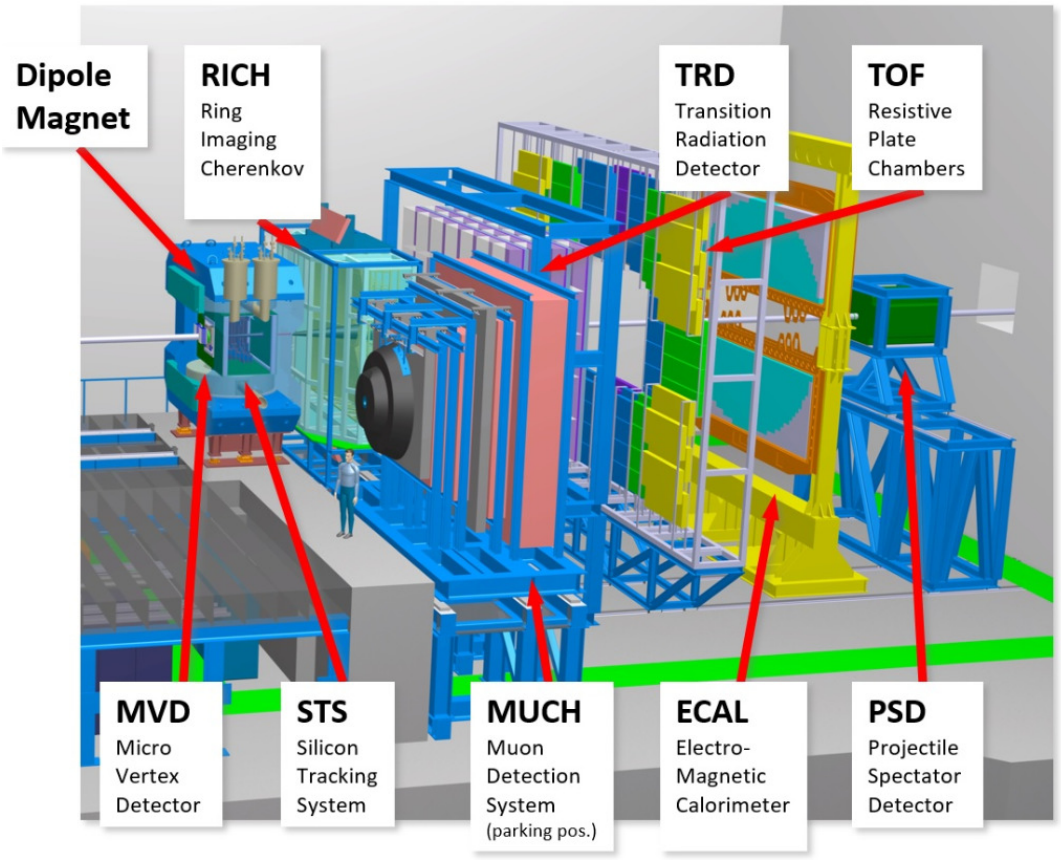

Figure 1.2: Model of CBM detector with sub-detector systems. The beam is coming from the left and hits the target inside the dipole magnet. Source:[TS18]

interaction point lies within a magnetic dipole field to allow tracking and momentum measurements. It is directly followed by a Micro Vertex pixel Detector (MVD) which identifies primary vertices. Located inside the dipole magnet is the Silicon Tracking System (STS), the main momentum reconstruction sub-detector of CBM. Like the MVD it is based on silicon technology to match

the required radiation hardness and high spacial resolution. It is build as a double sided strip detector. The Ring Imaging Cherenkov Detector (RICH) and the Muon Chambers (MUCH) located behind the magnet are interchangeable. Depending on the experimental focus on electrons or muons one can use the corresponding detector. The Transition Radiation Chamber (TRD) serves as intermediate tracking point. It measures the energy loss of particles over distance allowing for additional particle distinction. Located behind the Time-of-Flight wall (TOF) are the Electro-Magnetic Calorimeter (ECAL) and a Projectile Spectator Detector (PSD). The ECAL system is built of 124 alternating layers of scintillating fibers and lead absorbers. Its energy measurement will improve the Particle Identification (PID) capabilities of CBM. PSD is a hadronic calorimeter with 60 layers. It will observe beam ion fragments from the interaction to determine the centrality of the collision.

The main PID sub-detector is the TOF wall consisting of Multigap Resistive Plate Chambers (MRPCs). Measuring the time of flight of a particle from the Vertex to the detector allows the determination of its mass, if its momentum is known from tracking through STS and TRD. Hence, identification of the particle is possible. To achieve the required separation power one prerequisite for TOF is a time resolution better than 80 ps while covering an area of 120 m^2 and coping with incident particle flux rates between 0.1 kHz/cm^2 and 100 kHz/cm^2[DH18].

The development of MRPCs consisting of glass which will be used in the intermediate and outer regions of the wall has been conducted by groups in China at Tsinghua University (THU) and University of Science and Technology China (USTC). Testing of the detectors and assembling them into modules is done at the Physikalisches Institut of the University of Heidelberg and currently ongoing. As part of the FAIR phase 0 program which is intended to install and operate detectors for CBM in existing experiments the TOF-detectors will be installed in two projects. On the one hand 36 modules will be placed on the east pole end cap of the STAR detector to extend its PID capability beginning operation in February 2019. On the other hand 5 modules will be part of the miniCBM setup at GSI which aims to synchronize data readout and processing of the different sub-systems of CBM in a small fashion[DH18].

1.2 Motivation

The testing of MRPC-modules with cosmic rays to determine their efficiencies and time resolution is currently ongoing in Heidelberg. The test stand consists of several detectors layered above each other to allow for tracking purely with MRPCs. A graphical representation of this setup in a 3D-model is provided by an event display which can be used to observe individual events. The objective of this thesis was to provide additional functionality and information to this display to enable the user to understand the observed detector responses and functionality of the analysis software.
Therefore, chapter 2 starts with the physics of forming a signal in the detectors. It is explained which test setup was used and how the data was read out. Chapter 3 gives an overview of the analysis software and explains the additional functionality for the event display that was provided within the scope of this thesis.
In addition several applications of the new functionalities are studied in chapter 4. This demonstrates the benefit of an event display as a quality assurance tool. Finally, chapter 5 summarizes the results and gives an outlook to further uses of the event display.

2 Experimental setup and physics background

2.1 Particle interaction with matter

To measure physics observables in experiments it is necessary to understand how particles interact in the detector to form a signal. Different particles interact with matter in different processes, depending on their energy. For most detectors electromagnetic interactions are the dominant part for particle energy loss. In the following section, interactions between particles heavier than an electron with matter are discussed as they occur in the MRPCs, as well as interactions of electrons with matter. Interactions of photons will be mentioned briefly.

2.1.1 Ionization energy losses for heavy charged particles

In the process of ionization particles interact with the atomic shell of the medium they are passing through. Energy loss occurs due to ionization and excitation of shell electrons. The incoming particle scatters inelastic with the electron shell. Due to their heavy mass the particles stay on their trajectory. The energy loss over distance arises from the ionization of many electrons with a small loss ($\approx 10\,\mathrm{eV}$) in every ionization process. This can be characterized by the Bethe-Bloch formula (in natural units $\epsilon_0 = c = \hbar = 1$) in its relativistic form:

$$-\frac{dE}{dx} = 4\pi \cdot \frac{z^2\alpha^2}{\beta^2} \cdot \frac{Z\rho}{Am_N m_e} \cdot \left[\frac{1}{2} \cdot \ln \frac{2m_e\beta^2\gamma^2 T_{max}}{I^2} - \beta^2 - \frac{\delta}{2}\right] \tag{2.1}$$

With universal constants m_e as electron mass, m_N as nucleon mass, α as fine structure constant. Parameters of the incoming particle are its charge z in units of the charge quantum e, velocity $\beta = v/c$ and gamma factor $\gamma = (1-\beta^2)^{-1/2}$. Additionally, properties of the medium like charge Z and atomic number A of the media atoms, density ρ and average ionization energy I contribute. δ is a small correction due to polarization of the medium. It is very small for gases and therefore negligible. T_{max} is the maximal energy deposit in one collision. For particles much heavier than the electron holds $T_{max} \approx 2m_e\beta^2\gamma^2$.

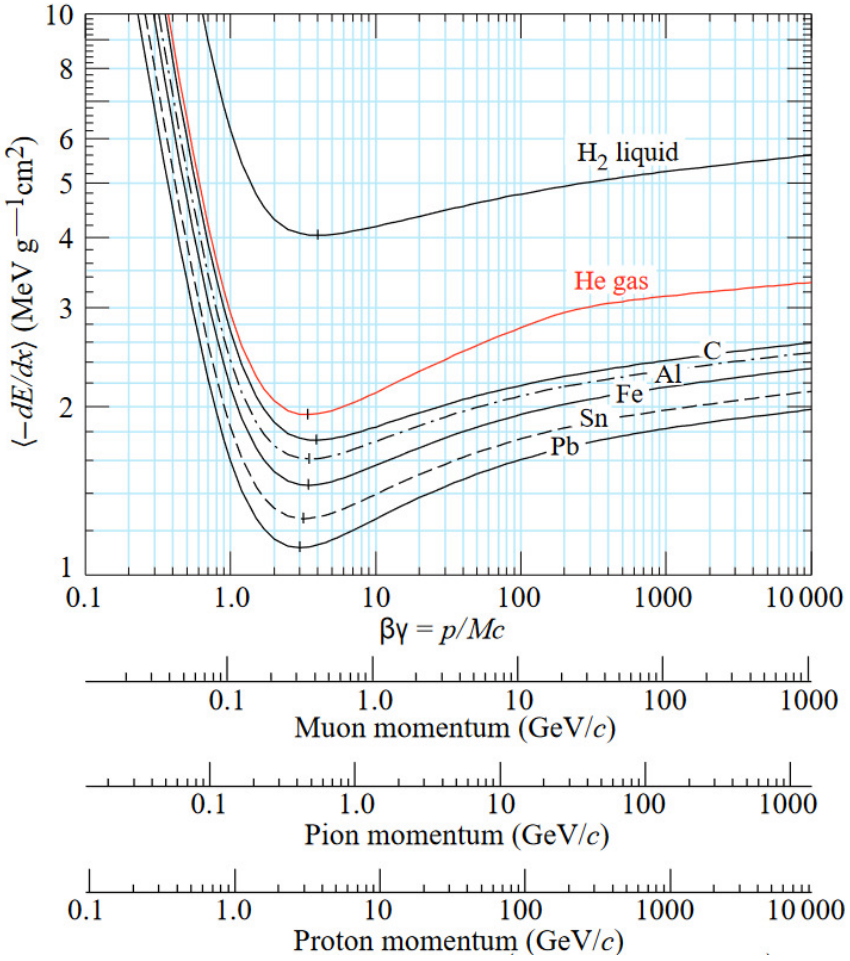

Figure 2.1: Bethe-Bloch curve for different media. The particles follow an universal behavior with minimum ionization at $\beta\gamma \approx 3.5$ Source:[Tan+18]

The Bethe-Bloch formula exhibits an universal behavior for many different par-

ticles (see fig. 2.1). For small energies ($\beta\gamma < 1$) the energy loss is proportional to $\beta^{-5/3}$. In the region of $\beta\gamma \approx 3.5$ particles have minimal ionization capabilities and are therefore called Minimum Ionizing Particles (MIPs). With increasing energies there is a logarithmic increase in energy loss.

2.1.2 Energy loss for electrons

For light particles like electrons and positrons one cannot neglect the deflection of the trajectory due to scattering with the electronic shell. One can derive an adapted Bethe-Bloch formula which accounts for that. In addition, another effect arises for electrons which is called Bremsstrahlung. Deflection from the Coulomb-field of the atoms accelerates the light particle that therefore radiates a photon. For the energy loss over distance one finds

$$-\frac{dE}{dx} = \frac{E}{X_0} \tag{2.2}$$

with the so called radiation length X_0 which can be calculated from material properties.

2.1.3 Energy loss for photons

Interactions of photons with matter underly mostly three processes each dominant in a different energy range. For low energies the Photo-effect dominates where the photons is absorbed by an electron. For medium photon energies the Compton-effect occurs as elastic scattering of photons with quasi free electrons of the atom. For energies above $E > 2m_e c^2$ the photon can produce an electron-positron pair in the presence of a Coulomb-field.

2.2 Cosmic radiation muons

Cosmic rays are high energetic particles reaching earth originating from outside the solar system and even distant galaxies. Cosmic radiation consists mainly of protons that scatter on the atomic nuclei of earth's upper atmosphere on their

way to earth.

$$
\begin{aligned}
p + p &\rightarrow p + n + \pi^+ \\
p + n &\rightarrow p + p + \pi^- \\
p + p &\rightarrow p + \Lambda(\rightarrow p + \pi^-/n + \pi^0) + K^+
\end{aligned}
$$

These reactions form pions and kaons which can decay further into muons:

$$
\begin{aligned}
\pi^+ &\rightarrow \mu^+ + \nu_\mu \\
\pi^- &\rightarrow \mu^- + \overline{\nu}_\mu \\
K^+ &\rightarrow \mu^+ + \nu_\mu
\end{aligned}
$$

The ratio of positively to negatively charged muons is about 1.25. The incoming flux at sea level is about $100\,\frac{\text{particles}}{\text{m}^2\cdot\text{s}\cdot\text{sr}}$. The muons reach earth's surface before decaying only because there is time dilation due to their highly relativistic nature. The energy distribution of the muons peaks at about 1 GeV with an average kinetic energy of 2 GeV (see fig. 2.2).

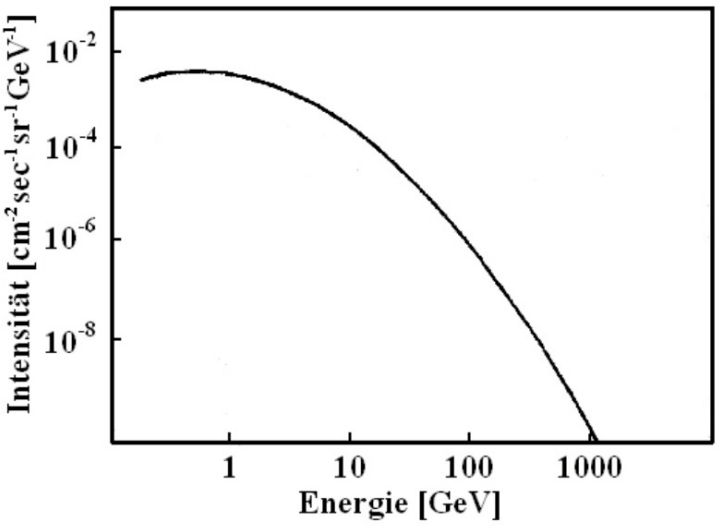

Figure 2.2: Energy spectrum of cosmic muons at sea level. Source:[FP1]

Since they are not subject to strong interaction muons loose their energy mainly due to ionization according to Bethe-Bloch.

The mean lifetime of the muon is $\tau = 2.197\,\mu$s following an exponential decay law. They decay via weak interaction:

$$\mu^+ \rightarrow e^+ + \overline{\nu}_\mu + \nu_e$$
$$\mu^- \rightarrow e^- + \nu_\mu + \overline{\nu}_e$$

2.3 Resistive plate chambers

The detectors for the ToF-wall of CBM consist of Resistive Plate Chambers (RPCs). In the following their working principle will be explained.
RPCs are gaseous detectors that stand out due to a very good time resolution ($\sigma_t < 80\,$ps) and high efficiency ($\epsilon > 95\%$) while being comparably cheap in production. In its simplest form a RPC consists of two high voltage (HV) electrodes with a gas filled gap between them. An incoming particle ionizes the gas and produces electrons. In the electric field between the electrodes these electrons are accelerated and form additional electrons and photons. An avalanche of charged particles develops, inducing a signal in special readout electrodes.
If a discharge channel would form it would leave the detector insensitive to other particles until the electric field recovers. To prevent this from happening, glass electrodes with a conducting layer on the outside for applying HV are placed next to the gas gap. They provide a high resistance ($\rho \approx 10^{12}\,\Omega$cm) so the field collapse only occurs locally and recovers more quickly. The presence of the avalanche at the glass electrode induces a signal in the readout-electrodes. In order to be transparent to the induced signal the conducting layer for HV is also made from a highly resistive material.
RPCs are used in two different application areas depending on the developing avalanche. If the avalanche grows so big that also photons are present in it, one speaks of "streamers". So called Trigger-RPCs develop these streamers and are used as a trigger in multiple experiments. Preventing the development of streamers leads to Timing-RPCs. They are used for the time-of-flight method due to a very good time resolution.
One can prevent the formation of streamers with different methods. Quencher-gases can be used to bind free electrons (in the case of sulfur hexafluoride SF_6)

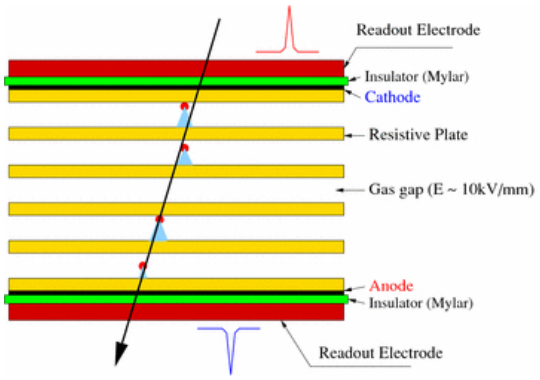

Figure 2.3: Structure of a Mulitgap-RPC. The resistive glass plates divide the gas volume in several gaps. A particle can form an avalanche in each gap inducing a signal on the readout electrode trough the glass plates. Source:[Sha+06]

or photons (with Isobutane), thus limiting the size of the avalanches. Bigger gap sizes and higher electric fields lead to an increased probability of streamers. They also influence the efficiency and time resolution of the detector.
One solution to maximize the performance of the detector and reduce the streamer probability are Multigap-RPCs (see fig. 2.3). The gas gap is divided into smaller gaps each separated by a glass-plate. Each gas gap is too small to produce a streamer but there are many gaps, leading to a high probability of an avalanche and thus high efficiency. One can build MRPCs in a double stack fashion where the electric field is applied between outer electrodes and one inner electrode. This doubles the number of gaps while providing the same electric field. A high electric field leads to fast growth of the avalanche and fast induction of the signal, thus improving the time resolution.

2.3.1 MRPC3a and b modules

For the CBM-TOF wall several MRPCs have been developed to suit the changing particle rates at different positions on the wall. For the intermediate and outer region double stacked MRPCs with 32 readout strips with a geometry of $1 \times 27\,\mathrm{cm}^2$ are planed. These prototypes are called MRPC3a developed at THU and MRPC3b developed at USTC. All measurements presented in this thesis were performed in a test setup consisting of these MRPCs.
MRPC3a has low resistive glass-plates and 2×4 gas gaps with $250\,\mu\mathrm{m}$ gap size (see fig. 2.4a). The glass has a thickness of $0.7\,\mathrm{mm}$ and a resistivity $\rho \approx 2 \times 10^{10}\,\Omega\mathrm{cm}$. They will be used in the intermediate rate region with

fluxes up to 5 kHz/cm^2.
MRPC3b is planned for installation in the low rate region with fluxes up to 1 kHz/cm^2. They consist of float glass with a thickness of 0.28 mm and 2×5 gas gaps with a gap size of 230 μm (see fig. 2.4b).
Both detectors have been tested with a gas mixture of 90% R134a (1,1,1,2-Tetrafluoroethane), 5% SF_6, 5% i-Butane.

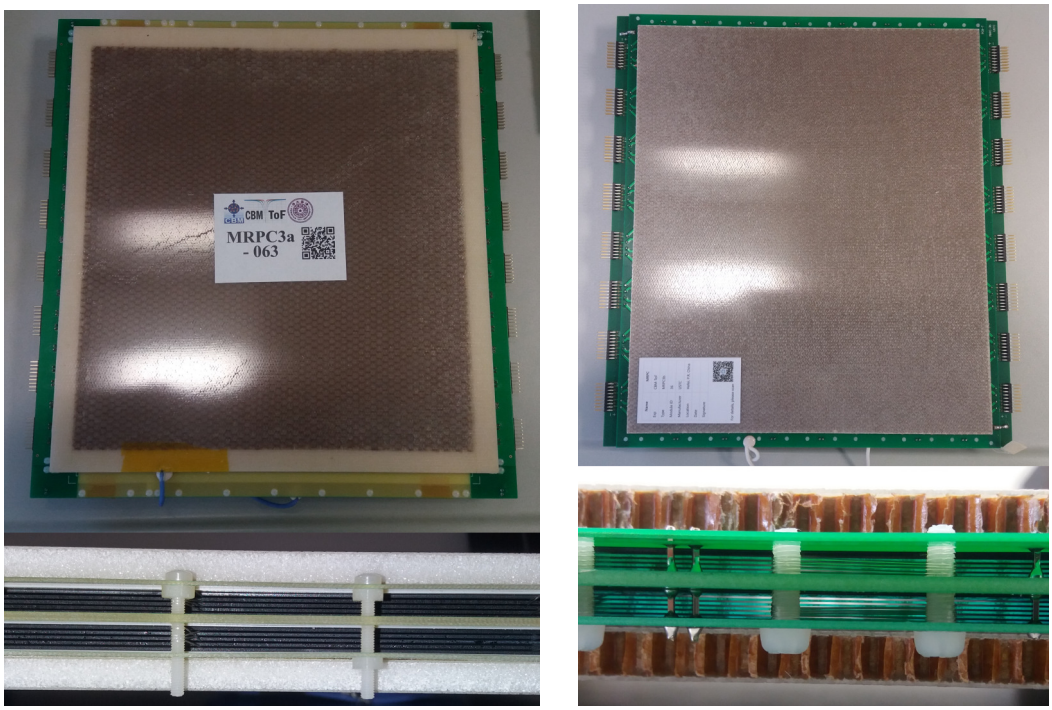

(a) MRPC3a **(b)** MRPC3b

Figure 2.4: MRPC prototypes for ToF. The pictures depict a top view in the top part as well as a side view of the detectors in the bottom part. There the individual glass plates become visible between the cover of the detector.

2.4 Cosmic test stand in Heidelberg

In order to test the MRPC prototypes which are foreseen to be build in modules for mCBM and STAR, a test stand with six detectors has been established in Heidelberg (fig. 2.5). Testing with cosmic muons allows to determine time-

resolution and efficiency with the use of data-analysis software written for ToF inside CbmRoot (see chapter 3.2).

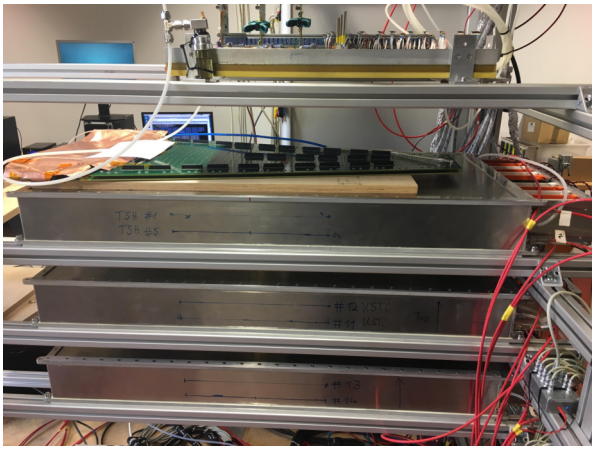

(a) three modules each containing two detectors centered in the middle.

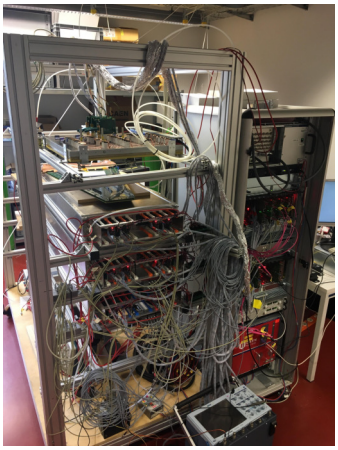

(b) readout electronics attached at the back-end of the modules

Figure 2.5: Test stand in Heidelberg where six detectors are tested with cosmic muons.

2.4.1 Readout and Data-acquisition

The induced signal on the readout electrodes originating from the avalanche is too small to be directly processed. Therefore a Preamplifier and Discriminator (PADI) is placed on each end of a readout strip. Figure 2.6 sketches functionality of the PADI. First the PADI measures the difference between the signal from top and bottom readout electrode. It then applies a threshold to the amplified signal and transmits a logical signal as long as it is above the threshold. This duration is called Time over Threshold (ToT). The amplification of the PADI is highly non-linear. The shape of the amplified signal in 2.6 doesn't represent the incoming signal into PADI and thus doesn't follow this exact shape. Likewise the relative height of the amplified signal to output signal is not realistic.
Located on the back-end of modules is the GSI Event-driven TDC with four channels (Get4) chip. Data cables from the PADIs are routed to one end of the modules where a backplate is mounted. This passes the data from the inside to Get4 on the outside. This chip extracts the start time of the signal (T0) and

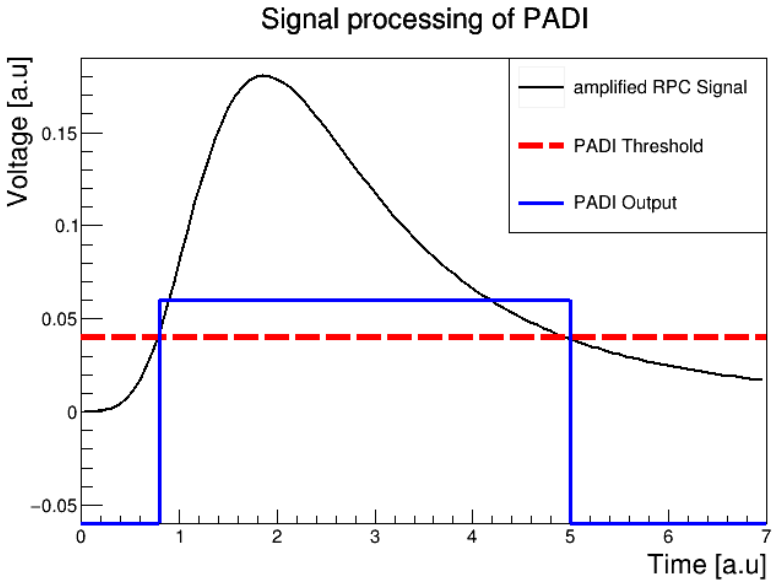

Figure 2.6: Sketch of signal processing of PADI. As long as the amplified signal is above a preset threshold the PADI transmits a signal.

the ToT as digital values from the PADI-signal. The modules tested within the scope of this thesis were equipped with PADI10 boards and Get4v2.0 chips.
Each of these components collects data from several channels and thus concentrates it. Via a copper cable the data is transported to the AMC FMC Carrier Kintex (AFCK) where a FPGA chip further concentrates the different channels of the detector.
After that the First Level event selector Interface Board (FLIB) builds time slices of several microseconds. In these time-slices all information of the detectors in a given time period are stored. In the near future an additional board with GBTx-chips, developed at CERN, will be included behind the Get4. It will transfer the data via an optical link and thus open the possibility to place further readout electronics outside the experiment cave as well as minimizing crosstalk and loss over distance.
The data can then be fed into the calibration and analysis software as described in section 3.2.

2.4.2 Geometry

The test stand used in this thesis consists of six MRPCs in three modules. A module is a gas filled aluminum box with two detectors inside which are arranged above each other. The readout of the detectors is routed to one end of the module (see fig. 2.5b). There, low and high voltage as well as gas are supplied to the detectors. The top module contains MRPC3a detectors from THU, the other two modules contain MRPC3b detectors from USTC. Figure 2.7 shows the geometry of the setup with corresponding detector naming. Two modules are 20 cm apart, the two detectors in the module have a spacing of 4 cm. In this way cosmic muons traverse through six modules (depending on their incoming angle) which allows for track reconstruction of the muons.

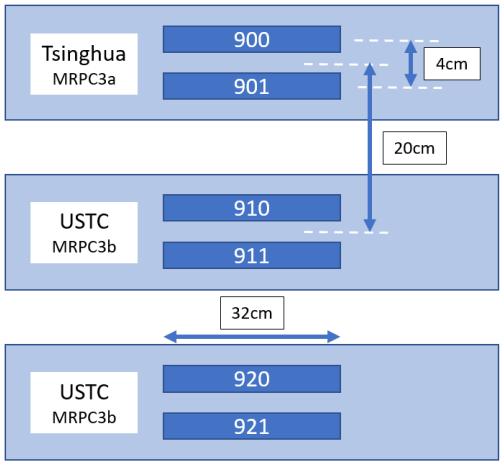

Figure 2.7: Geometry of the cosmic test stand. The top module consists of Tsinghua detectors, the other two of USTC. Modules are spaced 20 cm apart with a distance of 4 cm between two detectors. This view doesn't show the Y-direction of the setup.

2.4.3 Data run r0067

The data used in this thesis was taken in data run r0067. It was started on 9th of April 2018 and lasted for 22 h. This lead to about 600000 events.
All detectors were operated with an electric field of 112 kV/cm. For MRPC3a this corresponds to a applied high voltage of 5600 V and for MRPC3b 6400 V. The threshold was set to −300 mV for THU-detectors and −165 mV for USTC.

Under these conditions the time resolution of the detectors were found to be $\sigma_t \approx 60\,\text{ps}$ while having efficiencies of $\epsilon \approx 95\,\%$ as will be presented in the

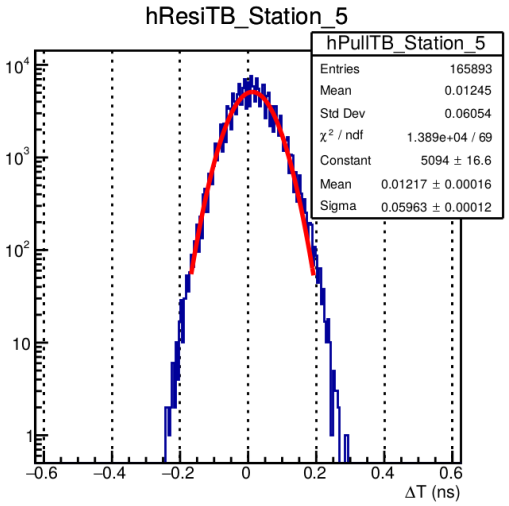

Figure 2.8: Distribution for detector 920. For every track of multiplicity 6 a fit is performed without including the hit in this detector. The difference between fitted time and hit time is plotted on the X-axis. The sigma of this distribution represents the time resolution.

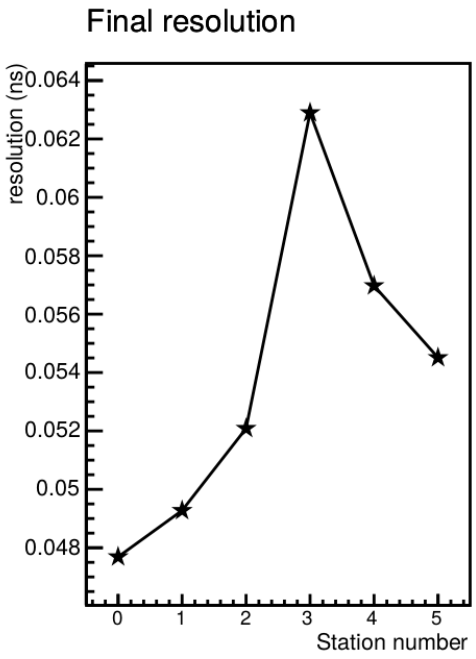

Figure 2.9: Time resolutions of all detectors ordered according to tracking setup 1 (tab. 4.1).

following. As an example figure 2.10c represents the spatially resolved efficiency of detector 901. It is homogeneous with a small loss in efficiency on the sides of the detector which is as expected. The overall efficiency was found to be 96.5%. 2.10a displays the hit position on detector 901 of tracks that left a hit in every detector layer. Since the setup consisted of 6 detectors these tracks have a so called hit multiplicity of 6. 2.10b depicts the expected hit position on 901 of tracks with multiplicity 5. These tracks left a hit in every detector but 901 and are considered to be inefficient for 901. From the fit of the track the hit position on detector 901 is extrapolated. The inefficiency is determined by the ratio of missed to found plus missed tracks.

An example for determination of time resolution can be found in figure 2.8. The sigma of a fitted gaussian represents the time resolution which is shown in 2.9 for all detectors ordered according to tracking setup 1 from table 4.1. The outer detectors (900=0 and 921=1) seem to be better performing than the

middle detectors. This is probably due to a bias in the analysis software. In general the time resolution of detectors is better if they are at the first two tracking positions. Therefore the testing of detectors is most reliable if they are placed in the middle of the setup. All detectors have time resolutions better than $\sigma_t < 64\,\text{ps}$ and fulfill the requirement for CBM.

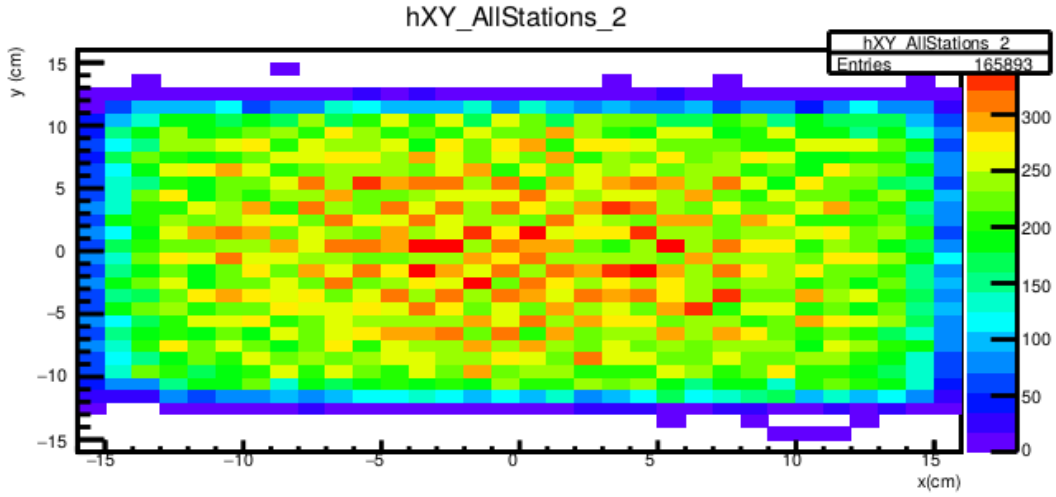

(a) all tracks of multiplicity 6 spatially resolved in 901

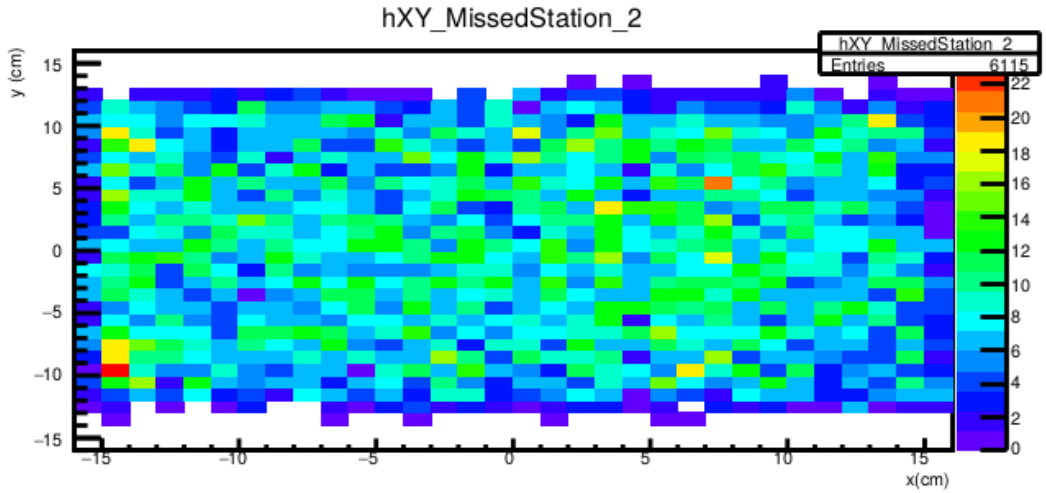

(b) missed hit in tracks of multiplicity 5 for 901

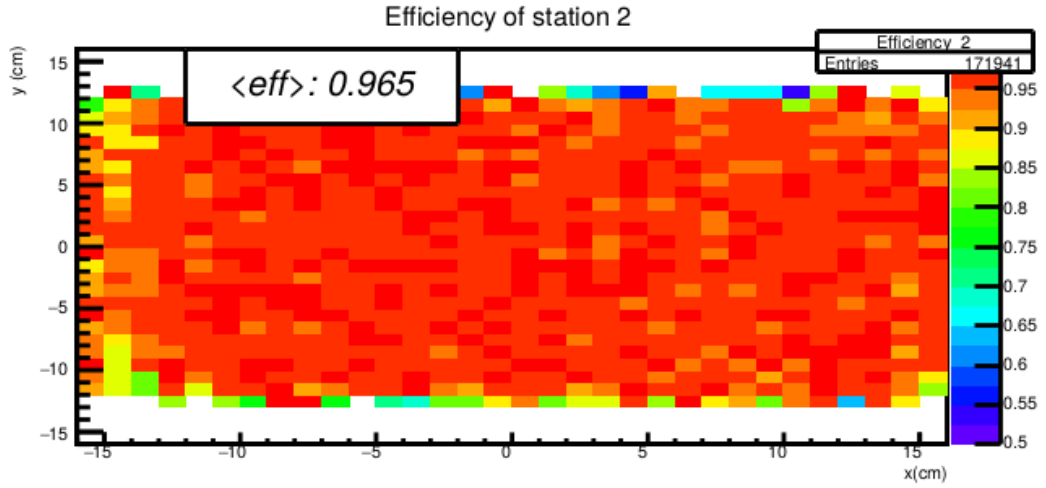

(c) space differential efficiency of 901

Figure 2.10: Efficiency of detector 901. The X-axis depicts the strip, y is measured along one strip. The efficiency is determined for each position from the ratio of missed hits to all tracks. The overall efficiency of 901 was found to be 96.5%

3 Software framework

In the following chapter the software framework in which the analysis of the cosmic data is performed and the event display is used will be explained. An overview of the different steps in the data analysis will be given. In addition the functionality of the event display will be presented. It will become clear what programming tasks were performed within the scope of this thesis.

3.1 Software framework

The statistical analysis of data taken by modern accelerator experiments requires software that can handle big data and provide visualization tools. For this purpose ROOT[Ant+09] has been developed at CERN as a modular scientific software framework and has since seen common application in many particle physics and heavy-ion experiments. For the CBM experiment two extensions to ROOT which offer special classes for data handling and hit building suited to the experiment exist. FairRoot offers the software framework in which experiments at FAIR can execute their analysis steps. CbmRoot contains the data structure of the experiment, for example with classes for hits on the detector or reconstructed tracks.
The main element of FairRoot is the so called FairRootManager. It is defined in the execution macro of the analysis and manages the different tasks one wants to perform. Every task that has to be done in data processing like building tracks from given hits, is built as a FairTask. It contains an Exec-function in which its action is performed (in this example the tracking) and it is added to the FairRootManager. By calling the Run-method –starting a FairRun– of the Manager, data reading is started and the different assigned tasks will be performed.

3.2 TOF data processing

For processing the data of the ToF detectors several classes and tasks have been developed and are being used in the analysis of the cosmic data from the test-stand in Heidelberg. Figure 3.1 sketches the individual tasks performed during a typical analysis run.

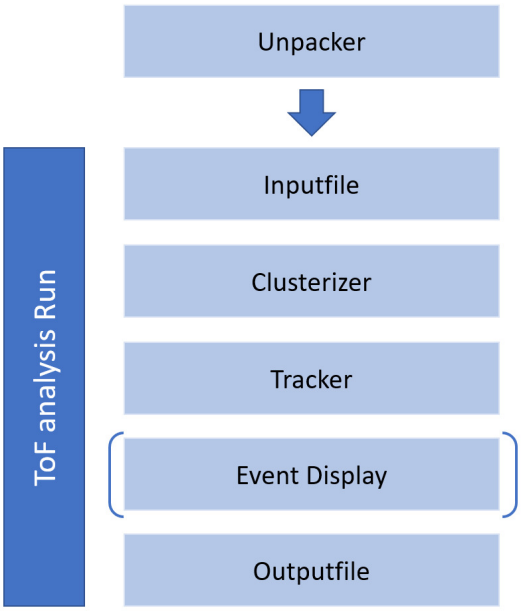

Figure 3.1: Typical ToF analysis chain. The unpacker builds the data file which will be used in the FairRun. The Clusterizer builds hits from the data and the tracker combines hits originating from the same particle to one track. An event display or other classes can be used after the tracker. The outputfile also includes all QA histograms produced during the analysis.

3.2.1 Unpacker

The first step is the Unpacker which takes the raw data and adapts it to FairRoot. The information from one detector signal is stored in the CbmTofDigi class which contains the detector address, time and ToT of this signal. In this task, events are generated which contain the information of all signals from the different detectors originating around the same time. In the cosmic tests these events have a length of 50 ns. They usually contain one, sometimes multiple particles, passing the detector setup. The Unpacker writes the data into a tree which is a data structure commonly used in ROOT and FairRoot. The tree contains a branch with events that themselves are arrays of CbmTofDigis.

3.2.2 Clusterizer

In the next step hit building from individual digis is done in a task called Clusterizer. For the cosmic test stand the CbmTofCosmicClusterizer developed by Prof. Dr. Norbert Herrmann has been used. A CbmTofHit is a hit on one of the detectors with position and time information. It exists of at least two digis since the signal in the MRPC travels to both sides of the detector and is read out individually. In addition the avalanche can induce a signal in more than one strip in which case one would like to merge the information of the relevant strips. The number of strips involved in a hit is called clustersize. An important parameter is the cluster-building-radius which defines how far away a digi can be in time and space and still be merged to one hit. The parameter is passed to the Clusterizer in ns and directly corresponds to the maximal allowed time difference between the digis. The maximal distance on the Y-position is determined as

$$\text{maxYDist} = \text{maxTDist} \times \text{SignalSpeed} \times \frac{1}{2} \tag{3.1}$$

Here, the signal speed on the readout electrodes is around 18 cm/ns. In X-direction –across the strips– only the neighboring strips are investigated for possible merge-candidates. After adding a digi into the cluster X,Y and T are set as the weighted mean of the participating digis. Further merging compares the distance between mean and new digi.
The determination of the position of a hit differs for every direction. Along the beam-axis or particle trajectory (the Z-axis) one knows where the detector is mounted and therefore its position. Since the position is fixed one does not have a relevant uncertainty. Across the strips (the X-axis) one knows which strip picked up the signal. Assuming a flat distribution for the probability where the signal originated across one strip the resolution is given by the strip width divided by $\sqrt{12}$. If more than one strip picked up parts of the signal the position is given by the average of the strips weighted with the signal strength. Along the strips (the Y-axis) the position and uncertainty are determined from the difference in time on both sides of the detector and the signal speed on the readout electrodes.

During the Clusterizer-process several calibrations are being applied to the data. Among others they concern an effect called time walk. A big analogue signal coming to the PADI has a steeper rise than a smaller one. Therefore it crosses the threshold earlier. Since this moment is used as time for the hit there is a systematic dependence of T0-time to the signal strength (ToT). Another effect comes from different electronic delays and cable length of each strip. This shifts the calculated center of the strip and thus prevents matching of position to the laboratory framework. Since these corrections depend on parameters like the cluster-building-radius they have to be applied in an iterative fashion starting with wide cuts and narrowing the cuts until the calibration converges. The output of the Clusterizer is a tree containing now arrays of CbmTofHits as well as histograms for quality assurance (QA) and calibration. In a CbmTofHit the time and position, cluster-size and ToT are stored.

3.2.3 Tracker

The final step in the data processing allowing determination of time-resolution and efficiency is the tracking. CbmTofHits of each detector layer are merged into CbmTofTracklets which represent one particle traversing the setup. The test stand in Heidelberg measures incoming cosmic muons. Since no magnetic field is applied they leave a straight line in the detector setup. To reconstruct hits to a track a tracking-algorithm has been developed by Prof. Dr. Norbert Herrmann.
The algorithm starts by taking two hits in different layers and fitting a straight line through them. This is called building a tracklet seed. It then looks in other layers for possible hits that can be merged to this tracklet because their residual to the track in space and time is smaller than a predefined cut value. When a hit is merged to the track the straight line fit is repeated. In this manner the algorithm builds bigger tracks until all detector layers have been taken into account. It is not restricted to finding tracks that leave a hit in every detector layer.
The order in which the detector layers are used in building the tracks is defined in the tracking setup. Tracking setup 1 from table 4.1 was found to be best

performing. It starts with the outer counters (i.e. 900 and 921 in the test stand setup, see fig. 2.7), because this allows for the best leverage to outliers. The tracking is performed iteratively with increasingly smaller cuts to exclude tracks with noise hits.
CbmTofTracklet is the class which represents a track. Among other information the tracklet velocity, theta angle in respect to the laboratory and goodness of fit are stored. The output of the tracker also produces QA histograms as well as histograms of different detector characteristics distributions.
The determination of the efficiency of one detector is done in the following way: A track leaving a hit in every detector except this one is considered to be inefficient for this detector. This number is divided by the number of tracks with hit-multiplicity (hMul) equal to the number of stations in the setup plus the number of inefficient tracks.

$$\epsilon_{Det} = 1 - \frac{\#tracks_{\text{all Stations but Det}}}{\#tracks_{\text{all Stations}} + \#tracks_{\text{all Stations but Det}}} \tag{3.2}$$

In order to determine the time resolution one only considers full tracks. For each detector one performs a fit without its hit contributing and then takes the difference between fitted time and measured time. In this fashion one fills a distribution of the differences for each detector (see fig. 2.8). The time resolution of one detector is the standard deviation of a gaussian fit to the distribution.

3.3 Event Display

An event display is a tool which allows graphical representation of the experimental data. Its applications range from high-level event visualization to debugging of simulations or reconstruction code as well as raw-data visualization[Gui]. It is embedded in ROOT as TEve-class based on the event display developed for the ALICE experiment. The functionality provides base-classes for rendering objects in a 3D-model. Each object can be modified by so called object editors and is presented in a list-tree. The functionality of the TEveManager allows management of the different elements and their interaction with

GUI-classes. Also the presentation of complex detector geometries can be handled by this tool.
TEve has been adapted and implemented in FairRoot. The main change comes in form of the FairEventManager replacing the TEveManager. This combines the event display functionalities with the FairTask system. Representing an object through a TEve-class requires a corresponding FairTask which adds it to the event display and the current FairRun. This allows the event display to access the data at different stages of the analysis chain. It also assures that the event display renders only one event at a time.

3.3.1 General functionality

Running an event display for the cosmic test stand was performed using a macro. In it the analysis with Clusterizer and tracking was performed before rendering an event. Unpacked data and the calibration histograms had to be provided to the macro. All parameters for the analysis could be defined inside the macro. Figure 3.2 reflects the GUI of the event display for one cosmic event.

The six detectors can be seen as semi-transparent layers in the main viewer. One particle is traversing all stations. It left a hit in all layers indicated by the cyan points. The reconstructed track is pictured by the vector. The color of the points and the track reflects the hit-multiplicity according to table 3.1. Hits that are not used to build a track appear as big red crosses.

hMul	3	4	5	6
color	green	blue	purple	cyan

Table 3.1: Color coding of the tracks in the event display

On the left side of the GUI are two menus. The upper one contains the list-tree of the different objects that are present in the event display. With the small tick one chooses to render or hide the selected object. The FairEventManager (highlighted dark blue in 3.2) is the relevant index tab which contains the rendered experiment data. The lower menu shows the editor of the current selected object. It is responsible for the graphical appearance of the object and

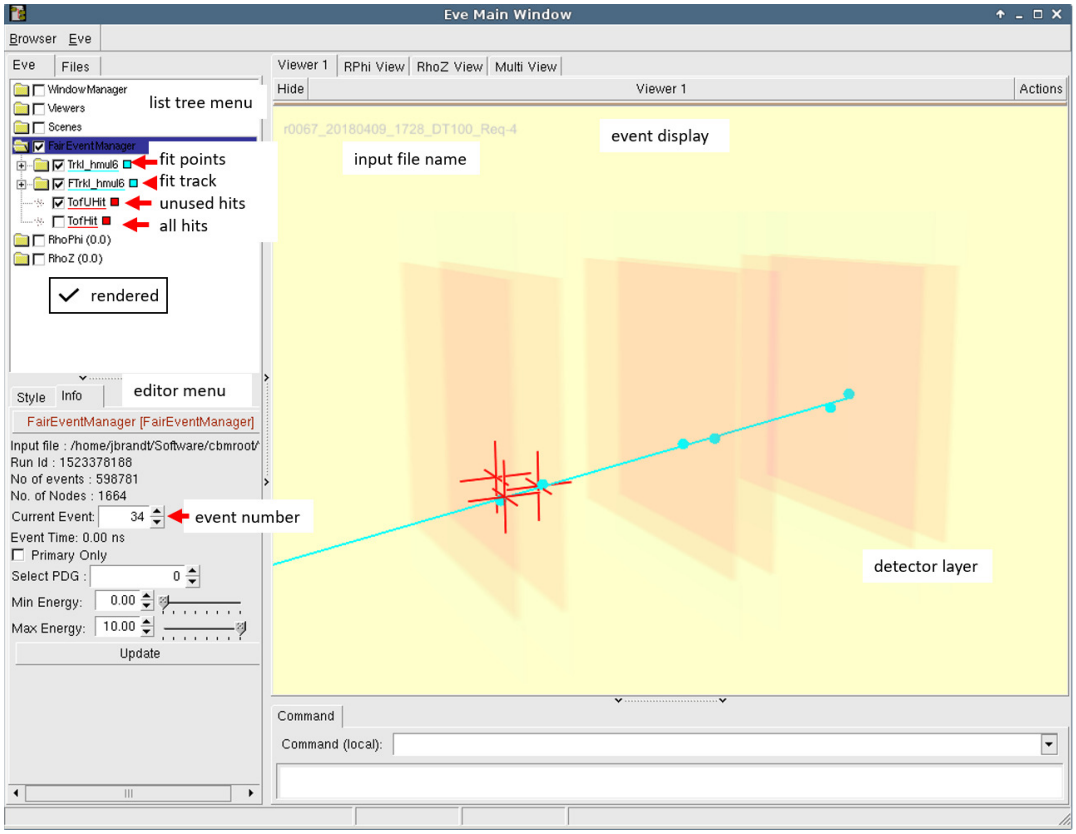

Figure 3.2: General functionality of the event display. It is divided into three sections. In the list-tree on the upper left one chooses which objects shall be rendered. The object editor on the lower left allows graphical changes to one specific object. Here it is chosen which event is displayed in the main window. This main window contains a 3D-movable model of the detector and the representation of the event hits and fitted tracks.

contains functionality to change the color of the track and many more. The editor of the FairEventManager shown in figure 3.2 provides the functionality to switch the current rendered event. Choosing a different event will trigger the FairRun to perform the tracking for the selected event and render it.
In this state of the event display it cannot efficiently be used as a debugging tool since not enough information is provided. Figure 3.3a illustrates such a case. The tracker found a track of multiplicity 5. But there is a hit in the missing detector layer which optically fits to the fitted track that didn't merge to the track. Together with the time information of the hit one could determine

if this led to the exclusion of the hit for this track. The scope of this thesis was therefore to provide such additional physical information to the event display in a graphical manner.
Additional observables that can be added to each hit are the time information and the ToT of the hit as well as the clustersize. For fitted tracks one would like to have measures to the goodness of fit. This includes the time and position residuals of the associated hits. To implement these features it was necessary to write several new classes that provided the needed functionalities.

3.3.2 Point Set Array

The most important information that was missing in the event display was the time information of the hits. The idea was to represent this observable in the color of a hit-marker. Displaying the hits had been done with a TEvePointSet which holds a number of points with their position information and displays them. Color, style and size of the markers were the same for all points so this class was not suitable anymore.
One alternative is a TEvePointSetArray, a ROOT class which is an array of TEvePointSets. In this class one sets a number of bins and a range for a distinction observable. Points are filled in the array according to this additional observable. This could be for example the charge thus grouping particles with the same charge in one graphical object. Each bin can have a unique color and marker. Especially, it is possible to color each bin according to a color palette with a gradient. The editor-class of this object provides a double slider for the observable. This determines which PointSets are rendered on the display. The observables for the Cbm-Tof event display could be the time or the ToT for example. This would color all points with hit-times in the same time interval in the same color which is a desired feature. But these points would be handled by one object so providing additional information in which they differ wouldn't be possible and require additional objects. Instead it was decided to distinguish the points by their unique ID which is saved in each CbmTofHit. Each point is now accessible in a TEvePointSet containing one point. A direct color coding according to time is not possible because the point IDs are not time sorted.

Instead the color has to be calculated from the time information.

3.3.3 Physics Information

For the color-coding a rainbow color palette with 50 colors was used. Although the rainbow color-palette should not be used for representation of scientific data because it introduces false gradients[RC], it was used because it provided the best distinction between useful hits that could be merged to tracks and late hits. To further improve the visual distinction of hit-times a sectional linear color scale was used. Table 3.2 illustrates the index of different colors in the rainbow palette.

Index	0	5-15	35	40	49
Color	purple	blue	green	orange	red
Time [ns]	0		3.5		50
ToT [a.u]	0	3			20

Table 3.2: Rainbow color palette

The hit time that is saved in a CbmTofHit is stored in nanoseconds with a clock cycle of about 32 h. This leads to hit times in the order of 1×10^{14} ns. To obtain useful numbers, the time of the first hit in each event was subtracted from all hit-times. In this frame the first hit starts at 0 ns and the last possible hit has a time of 50 ns as this is the length of an event built in the Unpacker. Since the first hit usually belongs to the particle leading to this event the majority of hits fall into the first few nanoseconds of the event. Only single late hits or noise hits have longer times. Most particles cross the detector setup with the speed of light as they are cosmic muons. The setup had a height of 44 cm and with $c \approx 30$ cm/ns they pass the setup in about 1.5 ns. Therefore the sectional linear scale interrupts at 3.5 ns. The first part is colored from purple to green (indexes 0 to 35) and the late times are colored from yellow to red (36 to 49) as shown in table 3.2. This leads to fact that a particle traversing the setup leaves a track which is usually colored from purple to blue whereby each hit-time can be distinguished. Hits that occur much later in the event appear yellow or red. Figure 3.3b depicts the same event as 3.3a with the new functionality that the

color of the hits is calculated from their hit time. The hits that belong to the track start in purple then change to dark blue in the middle module and then light-blue in the last module. This corresponds to a flight time of about 1.5 ns in the setup. The hit in the first detector that was passed has a yellow color. This corresponds to a hit time of 13.4 ns. In comparison to figure 3.3a one can now see that the missed hit appeared too late and therefore wasn't merged to the track.

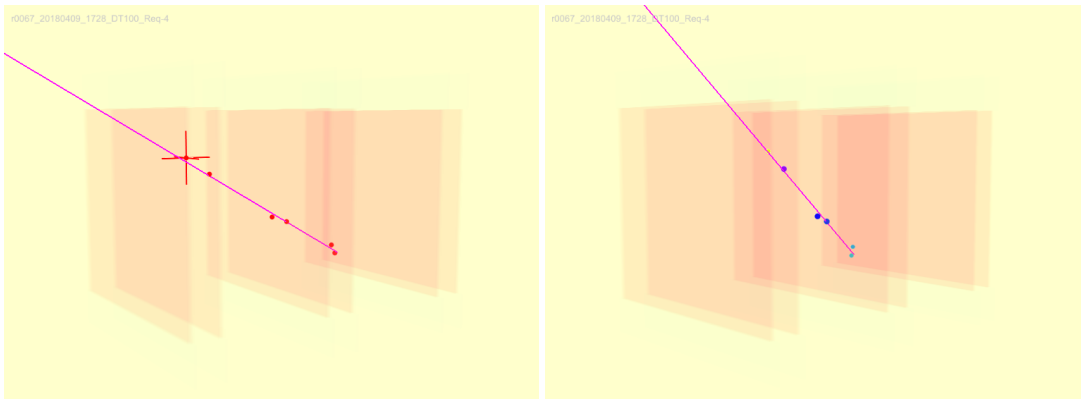

(a) old status **(b)** new event display

Figure 3.3: Event 15002 of r0067. Comparison of old and new functionality of the event display with a late hit as example. In the new time-colored version one can see, that the hit was detected too late and therefore not merged to the track.

The representation of time over threshold for a hit should also happen in a color-coded fashion. Since the ToT is corrected to have a mean of 5 due to different amplification factors on each PADI the ToT-values don't represent real ToT in nanoseconds any longer. Instead they are in arbitrary units with a maximum ToT of 20. For coloring the ToT the same rainbow color palette was used applied as a linear scale. In this way ToTs with 5 a.u appear in sky blue and the highest ToTs in red (table 3.2). For hits with clustersize greater than 1 the ToT reflects the mean ToT of all used digis. An example of hits in ToT coloring mode can be found in 3.6.
The third observable that should be provided for all hits is the clustersize. It was decided to reflect this quantity in the size of the markers that are used to display the points. The distribution of clustersize in all hits has a mean of

about 1.5. In theory clusters with a size up to 32 are possible when each strip is merged into one cluster. The size calculates according to:

$$\text{MarkerSize} = 1.25 + (\text{ClusterSize} - 1) \times 0.5 \tag{3.3}$$

This allows a visual distinction between different clustersizes while keeping the event display comprehensible even with big clusters (see fig. 3.5). The size of the clusters does not represent the actual size on the detectors in this configuration. This would be achieved with MS $\approx 4 \times$ CS. It nicely demonstrates that fitted tracks fit through all the adjoined points and how big a signal on the detector can be (see fig. 3.6). One disadvantage is that marker of the points are spheres and MS determines their diameter. Thus they reach into the Z-plane and overlap with other detectors which is not realistic since the signal is bound between the glass plates of the MRPCs and thus fixed in its Z-position. The big markers in 3.6 correspond to a cluster size of three. Even bigger clusters are not suited to be displayed in this modus.

3.3.4 Class structure

All of these different style modes can't be displayed at the same time. They are defined in the classes or set in the macro of the event display. Changing the appearance of the points while running the same event display is not possible in this way. To achieve this one needs a GUI-input in form of a drop-box or a button, much like the double slider for the TEvePointSetArray. This functionality is provided by the TEvePointSetArrayEditor-class which is automatically generated for each array. As this is a ROOT-class one cannot do custom changes to it. To solve this problem three classes where developed in the scope of this thesis providing these functionalities.
Figure 3.4 sketches the relations between these different classes. One needs a new class CbmPointSetArray that inherits from the TEvePointSetArray and comes with its own editor the CbmPointSetArrayEditor. A third class CbmPointSetArrayDraw is needed which is a FairTask. In this class one can generate a point set array and fill it with the relevant data from the analysis. The editor class contains two combo-boxes with a drop-down menu from which one can

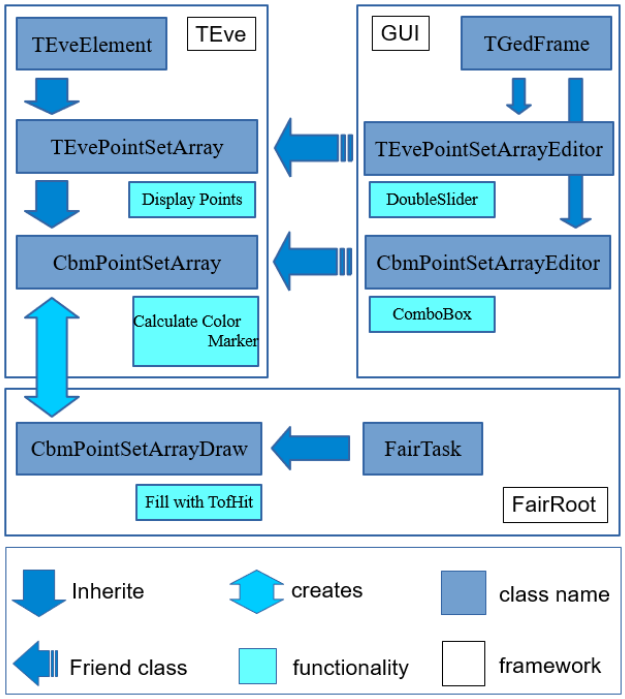

Figure 3.4: Class structure of the point set array. CbmPointSetArray is the object that is generated by the Draw-class which acts as a link to the FairTask system.
The Editor-class provides two Combo-Boxes and functionality to modify the appearance of the CbmPointSetArray.
These three classes were invented within the scope of this thesis.

choose the modus for color and marker-size. The boxes are located in the lower left menu like in figure 3.5 and 3.6. In the CbmPointSetArray the color and size is calculated from the time, ToT and clustersize which have to be provided for each point.
All three classes have the same two member variables called colorMode and marker-Mode. These are integer values each corresponding to one specific possibility of coloring and determining the size. Upon choosing an option from the Combo-Box the input is passed to the CbmPointSetArray. With a switch for color and size the corresponding methods are chosen.
Initializing the CbmPointSetArrayDraw-class in the execution macro of the event display one provides default values to color-mode and size-mode. In addition one specifies whether the ToF-hits are displayed on default when rendering a new event.

3.3.5 Additional event display functionality

There are four possibilities for coloring the hit marker. According to their hit time, ToT, point ID or all marker in red. One can choose these options from the Combo-Box for time in 3.6. For the size of the markers three options exist: Representing clustersize (eq. 3.3) or realistic occupation of strips or a constant clustersize as seen in 3.6.

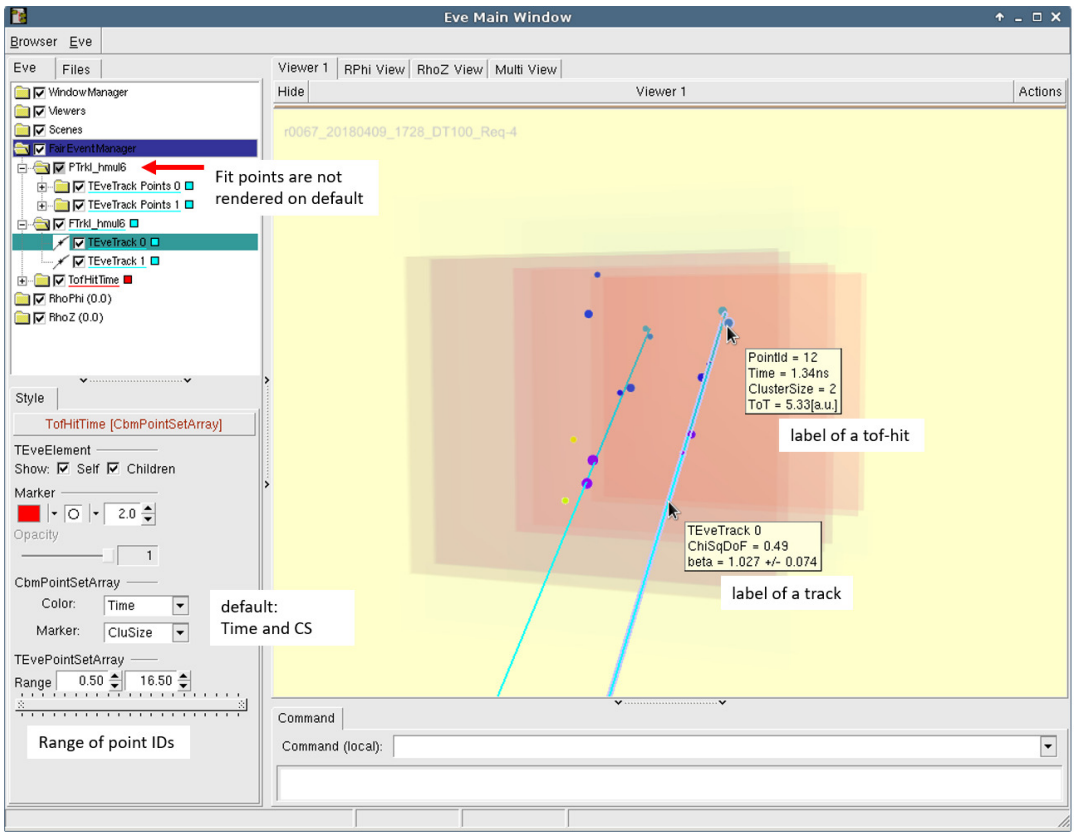

Figure 3.5: Additional functionality of the event display (1/2). The hits are displayed with time coloring and size calculated from the cluster size. The label information of tracks and tof hits is shown.

An additional feature that is provided with a TEvePointSetArray of ROOT is the so called BBox. This is a label that appears only when the mouse hovers above the object. Its content can be set by the user and present all relevant information. Since each point is uniquely addressable in the array it can have its own BBox. In it the point ID, time, ToT and clustersize are all shown with

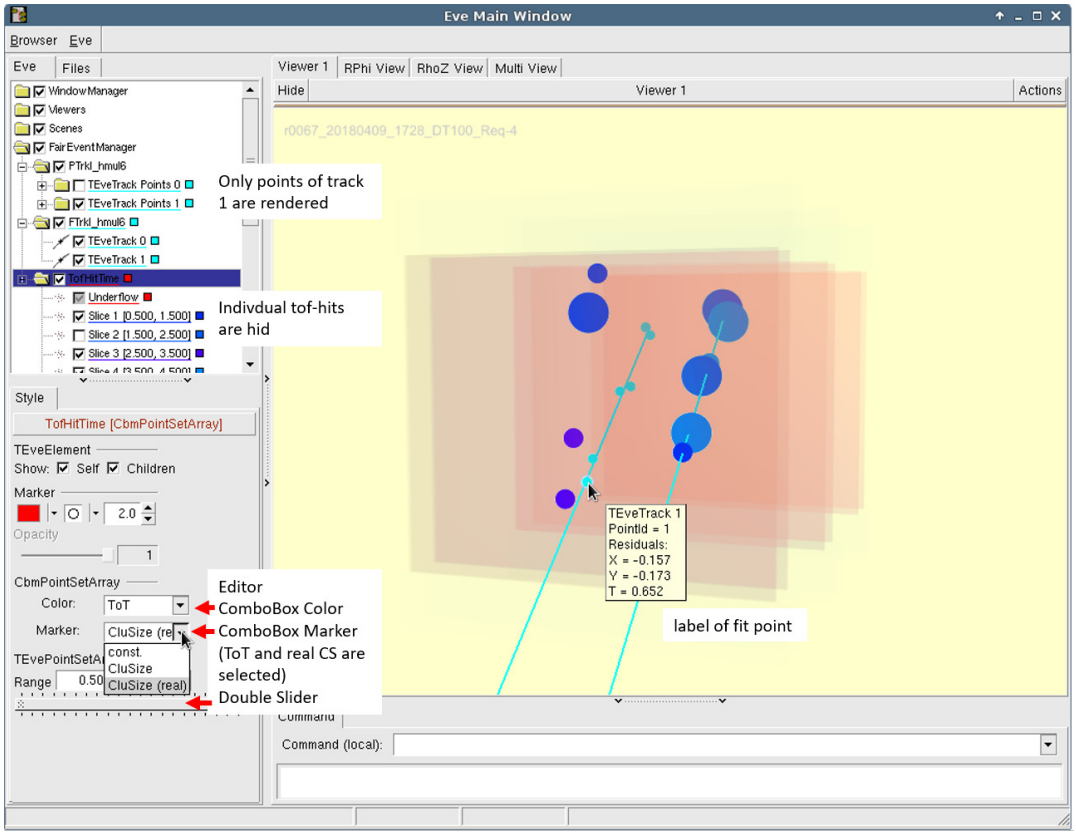

Figure 3.6: Additional functionality of the event display (2/2). The hits are displayed with ToT coloring and size representing the real size on the detector. The label information of a fit point is shown.

their number value as seen in 3.5.

3.3.6 Displaying tracks

The above mentioned class CbmPointSetArrayDraw is responsible for displaying all hits of the event and presenting their physical observables. This is all the information that is available after the Clusterizer. With the tracking one gets a new object that has to be presented: tracks and their corresponding hits. In the class CbmEvDisTracks the management of displaying all found tracks in an event is implemented. Tracks are grouped together according to their hit multiplicity and appear in the same color. For each track object which is responsible for rendering the vector there is a second object rendering the used

points. In this thesis this second object was replaced by a TEvePointSetArray to enable the use of a individual BBox for each point.
In the BBox of a track one first of all finds the ID of the track in this event. In addition the reduced χ^2-value of the straight line fit is shown. The third information is the velocity of the particle in relativistic units together with the error of this fit-parameter. An example is displayed in 3.5.
The BBox of the track points starts with a link to the track they belong to and their point ID to allow cross references to the points with the physical information. It then also contains the residuals of this hit to the track. They are calculated from the distance between measured and fitted value divided by the uncertainty. The residual of X and Y and time are displayed as they are used in determining whether a hit can be matched to a track. An example can be found in 3.6.

4 Applications of the event display

An event display has a wide set of possible applications. Most important is the visualization of the data to present it to people and to help understand the processes happening in the detector setup. Besides this it can be used in reconstruction-code and simulation debugging and other applications. In the following, cases shall be presented in which the event display functions as a debugging tool. In addition applications where the event display helps to understand the detector response to specific instances will be demonstrated.

4.1 Tracker debugging

As explained in chapter 3.2.3 the tracker requires the definition of a tracking setup in order to work. This setup contains the order in which the detectors are examined for possible hits that can be merged to a track.

detector	positions in tracking setup		
	1	**2**	**3**
900	0	0	0
901	2	2	4
910	3	3	2
911	4	4	5
920	5	1	3
921	1	5	1

Table 4.1: Detector position in different tracking setups. Setup 1 is usually used.

	χ^2_{red}	$\beta\,[c]$
setup 1		
track 0	2.72	0.961 ± 0.069
track 1	1.63	1.229 ± 0.245
setup 2		
track 0	0.91	0.907 ± 0.065
track 1	0.39	0.857 ± 0.127

Table 4.2: Parameters of fitted tracks in event 220.

4.1.1 Event 220

Event 220 in figure 4.1 represents a case where the tracking setup is a deciding factor to finding the "correct" track. 4.1a depicts the event for tracking setup 1 according to table 4.1. Two tracks were found. One with multiplicity 4 and one with 3. The corresponding hits are highlighted. Table 4.2 contains the label parameters of the found tracks. In both cases $\chi^2_{red} > 1.5$ which represents the bad visual correlation for the found tracks. Much better fitting seems a track which runs from the lower left to the upper right corner with a multiplicity of 5. Exactly this track is found with the tracking setup 2 from table 4.1 represented in 4.1b. Additionally a track with multiplicity 3 was found. The label parameters can be found in table 4.2. $\chi^2_{red} = 0.91$ for track 0 in 4.1b confirms that this is a better match compared to 4.1a.

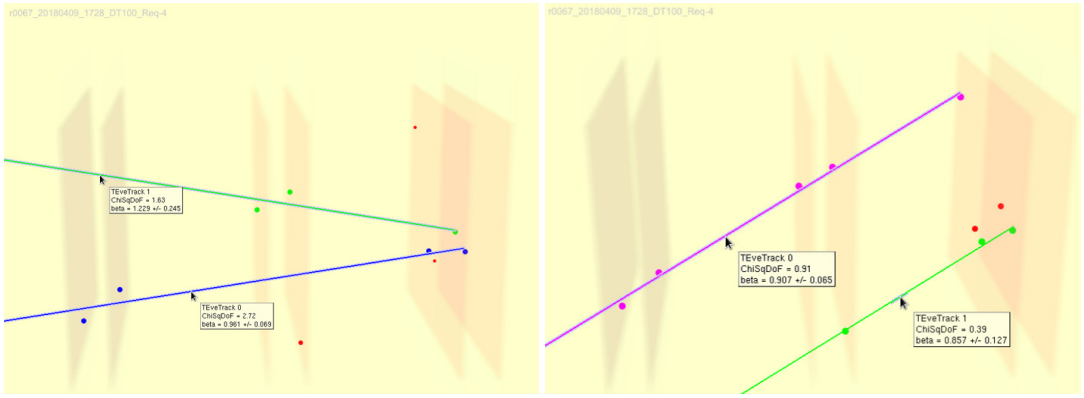

(a) χ^2_{red} for setup 1 **(b)** χ^2_{red} for setup 2

Figure 4.1: Event 220 of r0067. Depending on the tracking setup different tracks are found. The result of setup 2 seems more realistic which is supported by the smaller χ^2_{red}

The difference arises due to the tracking setup and thus the building of tracklet seeds. Both start with examining detector 900 which is displayed as the leftmost plane. In tracking setup 1 detector 921, the rightmost plane, is the next detector. It contains two hits. Next is 901 (second from left) with one hit. The tracker forms a tracklet 0 out of three hits containing hits in 900 and 901 as well as the better suiting in 921. The fitted line runs almost parallel in the lower detector half. The hits in 910, 911 and the upper one in 920 are too far away to

be merged. Instead the tracklet 0 is extended to multiplicity 4 forming the blue track. Since $\chi^2_{red} < 3$ the tracklet is accepted. Now the hits are not available for new tracks anymore. A new tracklet 1 is started with the remaining hit in 921. The next detector with a "free" hit is 910 at tracking position 3. This tracklet forms track 1 in the final step. Detector 920 is being investigated last in tracking setup 1 therefore the tracker doesn't build a tracklet seed containing this hit.
A tracking setup which forms the expected track with multiplicity 5 has to make sure that the hit in 920 in the upper corner is used in building a tracklet seed. Therefore tracking setup 2 has detector 920 on position 1. A tracklet seed containing the hit in detector 900 and the hit in detector 920 is being build. This tracklet expands through the detectors from left to right, picking up the matching hits. Detector layer 921 is being investigated last in this setup. It therefore cannot interfere with track 0 because this does not contain a hit in this layer. Extending the vector of track 0 one would see that it misses the detector layer of 921. From the remaining hits an additional track of multiplicity 3 was found.
Tracks of multiplicity 3 usually don't represent a cosmic particle producing a trace in the detector setup. The fitted velocity often exceeds the speed of light with a big uncertainty. The track 0 with multiplicity 5 on the other hand seems to originate from a cosmic muon. The hit in detector 921 is missing, because the track didn't traverse the detector in its active volume.

4.1.2 Event 397

Another example for the influence of the tracking setup can be found in event 397. 4.2a depicts the event with tracking setup 3. No track is found despite a good visual alignment. Using tracking setup 2 or 1 from table 4.1 the tracker successfully builds a track of multiplicity 4 containing all hits in the event. With $\chi^2_{red} = 0.41$ and a velocity close to the speed of light this track seems to originate from a real cosmic muon. If the tracker is not able to build a tracklet seed from the hits in the detectors of position 0 and 1 it can use hits from position 2 but not go further without a seed. Since position 2 in setup 3 is

detector 910 with no hit in it, the tracker is not able to build a tracklet seed.

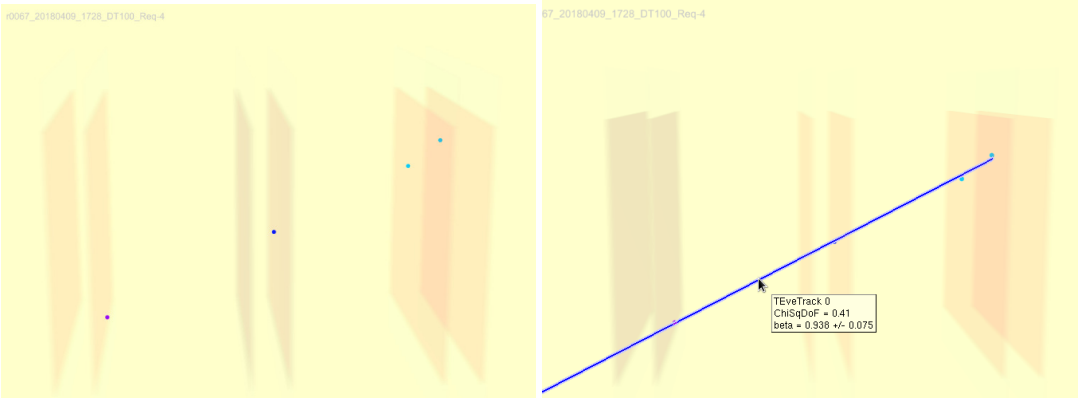

(a) Setup 3 **(b)** Setup 1 and 2

Figure 4.2: Event 397 of r0067. Depending on the tracking setup the tracker is not able to build a tracklet seed.

This only happens in events where two detectors didn't measure a hit either because they had been inefficient or the particle didn't traverse the active volume and missed the detector. This is rare and corresponding events are not used for determination of detector characteristics where tracks of multiplicity 5 and 6 are important.

4.1.3 Event 403

Event 403 depicted in 4.3serves as a third example. It is an event with 6 hits each in a different layer. Tracking setup 3 in 4.3a found a track of multiplicity 5 with the green hit in detector 921. Tracking setup 2 in 4.3b found a track with the light-blue hit in detector 920 and tracking setup 1 in 4.3c found a track of multiplicity 6 containing all hits.
The label parameters can be found in table 4.3. Including the green hit in detector 921 is not correct and leads to too high $\chi^2_{red} > 3$. The hit is off in the position to the track and is delayed by 1 ns in comparison with the hit in 920. This time delay also reduces the fitted velocity as can be seen in table 4.3.
Tracking setup 2 builds tracklet seeds with detector 900 (bottom in this view) and 920 (second from top). After that the detectors are examined from bottom

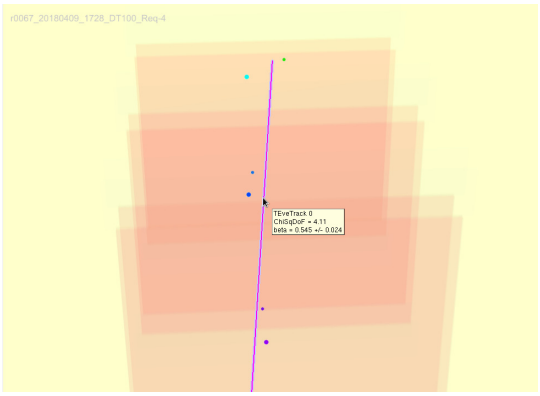

(a) Setup 3

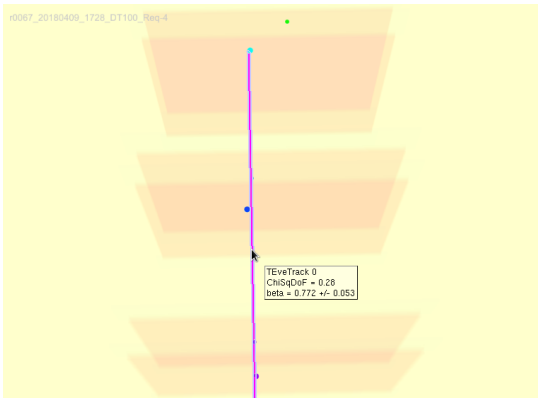

(b) Setup 2

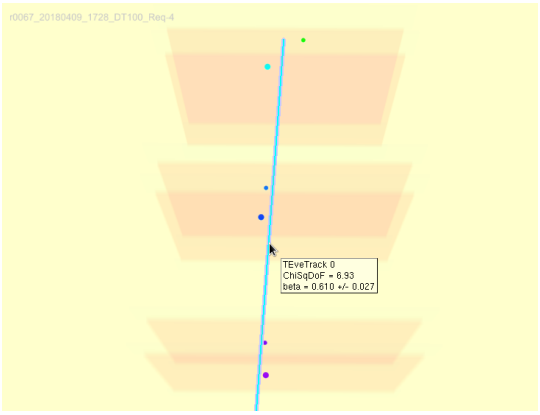

(c) Setup 1

	χ^2_{red}	$\beta\,[c]$
setup 1	6.93	0.610 ± 0.027
setup 2	0.28	0.772 ± 0.053
setup 3	4.11	0.545 ± 0.024

Table 4.3: Parameters of fitted tracks

Figure 4.3: Event 403 of r0067. Depending on the tracking setup different hits are used. In this event the tracking setup affects the multiplicity and therefore the efficiency of the detector.

to top with detector 921 being the last one. In this situation the hit is too far away in time and space to be merged to the track.
Tracking setup 1 and 3 build tracklet seeds from detector 900 and 921. The seed therefore contains the green hit. In setup 1 the detectors are examined from bottom to top. Adding a new hit tilts the fit more to the left. This is sufficient enough to also merge the hit in detector 920 which is taken into account last. No hit can be discarded from a track once it has been added. Therefore the hit in 921 remains part of the track despite a residual in X and T of $6\,\sigma$.
In tracking setup 3 detector 920 is on position 3. The current tracklet is pointing too far away in direction of the green hit to merge the hit to the track. The

other detectors that are examined after that are closer and are merged. No layer is examined twice for one track so the hit from 920 isn't merged at all.
In this event tracking setup 1 would have classified detector 921 to be efficient where it was not. In addition the time resolution of all counters is worsened because the fit is bad due to the inclusion of the hit in 921.

4.1.4 Conclusion

Tracking setup 1 is the setup which is commonly used in the analysis because it is proven to be best performing. Using the outermost detectors to build tracklet seeds allows for the biggest lever in building tracks and not including outliers from other detectors. On the other hand it has a systematical weakness in reconstructing particles that missed either the top or the bottom counter due to their θ-angle if the respective detector measured an additional hit from another source. This weakness is demonstrated with event 220.
Event 403 elucidates the leverage of tracking setup 1 which merges all points. This comes with the negative side-effects of worse time resolution and falsely improved efficiency of the outer detector in this event.
Every tracking setup has its strengths and weaknesses. Some parameters or special detector characteristics might not be calculated ideally by every setup. Therefore one has to choose the setup according to the task one would like to perform.
One observation is that detectors should not be used as seeds in the tracking setup if one wants to rely on the measured detector characteristics.
The amount of events in which the tracker doesn't find the "correct" solution is estimated to be around 1%. This estimation is based on consideration of several hundreds of events. It shows that for the majority of events the tracker is working properly. However, when going from 98% efficiency to 99% and higher efficiencies these effects could play a role.
There are also additional features one could add to the tracking software. One possibility would be to check for every hit after forming the complete track whether the matching criteria are still fulfilled. Another option could be to allow a hit to be merged in several tracks. In the end it would be decided to

keep the best track. Whether they improve the tracker significantly is not clear. One challenge of a tracker which is used in cosmic tests is the varying track angle. This is in contrast to a fixed target experiment where all primary tracks originate from one common point. Cosmic muons follow a $\cos^2$-distribution for their θ-angle. So the tracker has to be flexible and find tracks with all possible angles. This is taken into account by the use of the tracklet seeds from which full tracks are formed.
The tracker in its current state will only be used for the tests with cosmic muons where tracking of straight lines is sufficient. For later experiments like eToF at BNL or mCBM at GSI the ToF-system will only contain up to two layers. A useful tracking with this data alone is not possible despite having fixed target experiments where all particles don't cross each others trajectory. Instead the data of ToF will be combined with other detector systems like the STS in mCBM and final CBM. This silicon tracker system will provide many hits and thus allow tracking in the magnetic field (not present in mCBM). For this purpose a tracker based on the cellular automaton and Kalman-filter technique has been developed by groups inside CBM[AK16].

4.2 Big clusters

The distribution of cluster size depending on the strip of detector 911 can be found in figure 4.4. This histogram has entries filled up to cluster sizes of 10. The theoretically achievable cluster size is 32, if every strip contributes to it. The upper range of the histogram shown is set to 16 but entries above that are also observed as will be demonstrated.
The event display can visualize events with these big clusters. One can study whether such clusters appear multiple times in one event or if only one cluster is present in it. To find interesting events with big clusters a log-entry was written if the cluster size exceeded 10 in any counter for a given event. For data-run r0067, 142 big clusters were found in a total of around 600000 events. In the following event 59387 will be analyzed as an example. Figure 4.5a depicts the event in the display. The setup is rotated such that counter 921 is on the left and 900 is on the right. A cluster with cluster size of 23 was found in 921

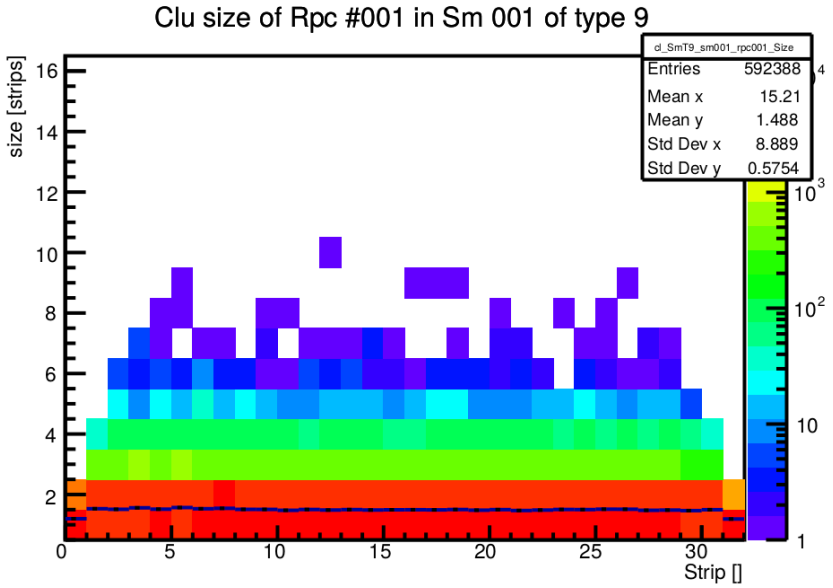

Figure 4.4: Cluster size distribution of detector 911 for each strip. The histogram range is set to 16 but even bigger clusters are possible and occur very rarely.

and a cluster of 17 in 911. In the other counters many hits are found with cluster sizes up to 5. The tracker found several tracks with hit-multiplicities of 5. On the first view it becomes clear that this event didn't originate from one cosmic muon. On the other hand one can see a color gradient in the time representation present through the detector layers. All of the hits in this event are time-correlated and passed the detector setup in wave-like fashion.
To find an explanation for this event behavior it is important to know whether the big clusters are real in the sense of a wide avalanche in the gas gap inducing a signal on many strips or if they originate from individual particle hits that got merged in the clusterizer due to their proximity in time and space. The relevant parameter that contributes to this is the cluster building radius (CBR, see chapter 3.2.2). The search for this event was done with CBR = 1 ns. This is a very large radius since it corresponds to about $20\,\sigma_t$. Values down to CBR = 0.3 ns are still very reasonable. 4.5b represents the event with CBR = 0.5 ns. The cluster in 921 split into two smaller clusters. The cluster in 911 stayed at the same size. The tracker found less hMul5-tracks but more with

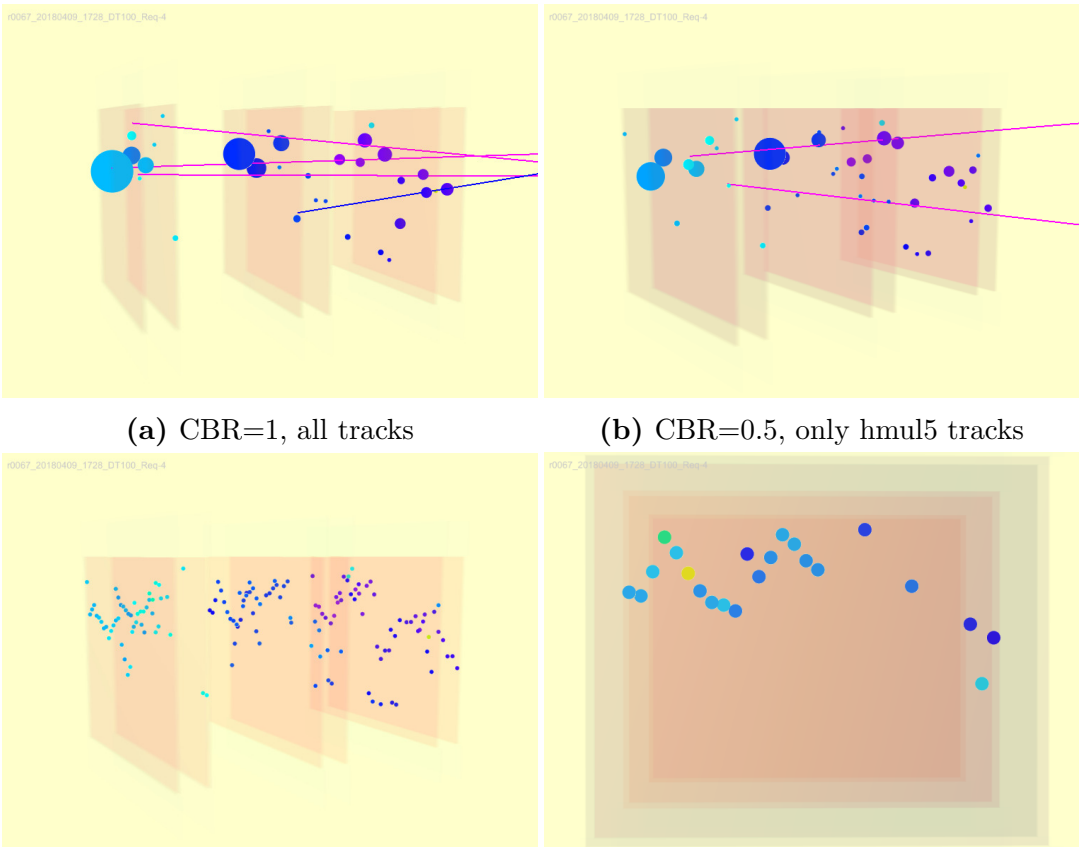

(a) CBR=1, all tracks

(b) CBR=0.5, only hmul5 tracks

(c) no cluster building and tracks

(d) hits in 911 in ToT-view and real cluster size

Figure 4.5: Event 59387 of r0067. Represented are different cluster building radii (CBR). The hits in the detector layers are time-correlated thus indicating a common origin.

hMul4 and 3 which are hidden in the picture. With this amount of hits and possibly crossing tracks the information from the tracker is not useful anymore in understanding the event. Figure 4.5c depicts the event in case of no cluster building at all. Here all found tracks were hidden. In this time representation of the hits the correlation between the detector stations becomes especially visible. It looks like a shower of particles went through the detector setup.

4.2.1 Cluster composition

Since in this picture all individual hits are rendered one can look at the contributions to one of the big clusters. This is depicted in 4.5d which shows all hits in detector 911 in ToT-color coding. The time difference between left and right hit that were merged to the cluster is 180 ps. The hits seem to follow a pattern which can also be spotted in 4.5c in detector 921 for example. Thereby each strip only has one hit.
This is reasonable since the detector can't distinguish almost simultaneous hits on the same strip. The position along the strip is determined by the different times the signal needs to travel to one side or the other of the detector. If another hit induces a signal in the strip while the signal of the first one is still traveling to one side the leading edge of the second hit might be merged with the first hit. This has several effects. The Y-position and hit time are calculated incorrectly because the arrival time on one side of the detector is wrong. In addition the ToT of the hit enlarges. The signals traveling to one side overlap and thus enlarge the time that the signal is above the threshold. This effect happened for hits on 911. One can see a green marker with ToT = 9.00 a.u and a yellow marker with ToT = 15.25 a.u. The light-blue markers correspond to ToT > 6.00 a.u. These hits thus have a higher than average (ToT = 5.00 a.u) ToT and may be composed of several primary hits in the detector. If one could distinguish them they would break the pattern and lead to a more clustered distribution of the hits.
The expectation for a big cluster that is produced from one particle would look differently. In the detector this would mean only one avalanche which is spread out in space so far that it covers several strips. In the center were it formed the highest ToTs would be measured and deviating to the sides the ToTs would be decreasing. This is not observed in 4.5d as the ToT stays around the same level over the participating hits.
Other explanations for this amount of hits at the same time could be a collective excitation of the gas or electronic reasons. In both cases one would expect a stronger alignment of the hits and the participation of the complete detector and not one half with full hits and some hits in the other half like it is the case

in the displayed event 59387.

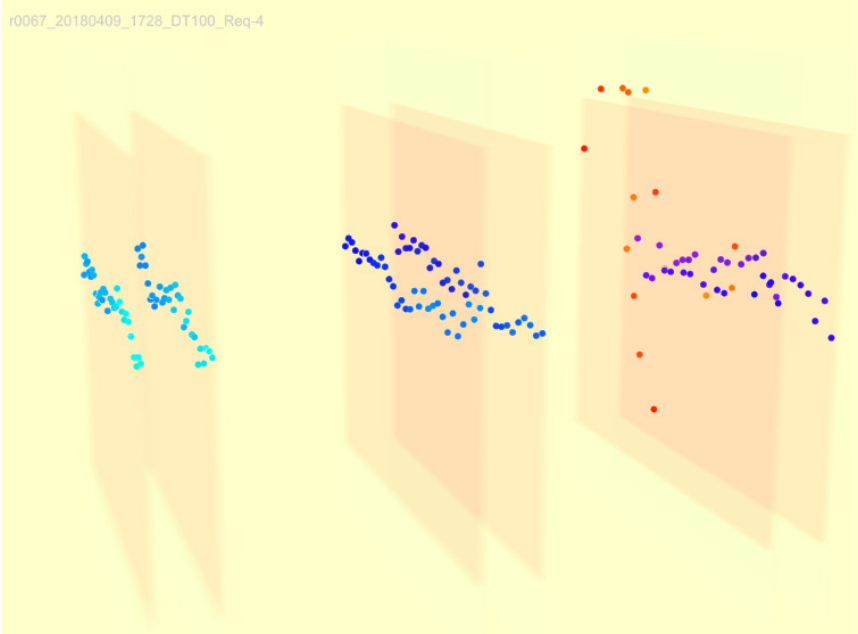

Figure 4.6: Event 503266 of r0067. With no cluster building it is visible that every channel fired strongly correlated in time and position. This is probably caused by electric charge up effects that erupted at the same time.

Collective electronic excitation could form from charge up effects of the test stand or spikes in the high voltage. The one example event that was found in run r0067 is displayed in figure 4.6. Almost every counter fired in 32 channels. In addition the hits are strongly time-correlated and placed in the middle of the strips.

4.2.2 Explanation of big clusters

The most probable explanation for the behavior in event 59387 is that the hits originate from different particles which traversed the detector setup at the same time. They could be a shower which was formed in the ceiling of the laboratory by an incoming muon.
The appearance of big clusters is due to the big cluster building radius. Merging these hits into one cluster is fine anyways since the tracker wouldn't be able to find individual shower particle tracks correctly. The tracks would rather

contribute to efficiency determination despite being unphysical. Thus having only one cluster prevents this.
142 big clusters (CS $>$ 10) were found in the data taken. Event 59387 is representative in its shape for many of the events with big clusters.

4.3 Search for Late Hits

Another kind of interesting events are late hits. In the past years it had been observed that there are tracks which seemingly have a hit in all detector layers. One of these hits would not be merged to the track because its time information didn't coincide with the fitted time. The detector detected this hit too late. This phenomenon should be studied with the event display.
The search for late hits was done with a log-entry of the tracker. An event was defined as containing a late hit if the tracker found a track of multiplicity 5. Further, in the missing detector layer had to be a hit with a residual in X and Y less than 3. An example of such an event can be found in 3.3b. The hit in detector 900 is about 13.6 ns too late.
Figure 4.7 shows time spectra of the late hits for detector 900 and 921 on different positions in the tracking setup. The X-axis depicts the time difference between hit time and estimated time for the detector from the fit.
The spectra were examined with different tracking setups which proved to make a big difference. For some positions a peak in the spectra at 0 ns appears. This means that the hit actually belongs to the track and should have been merged but for some reason wasn't. The height of this peak varies for tracking position 2 to 5. On position 0 and 1 it is not present. This is due to the fact that tracklet seeds are build from these two stations. If the track is merged with other hits successfully, then hits in counters on tracking position 0 and 1 are included definitely. One cut for this histogram was applied to the X- and Y-residual of the hits. They had to be less than 3. The χ^2-cut for hit matching is done with the quadratic added χ^2-value of X-, Y- and T-residual. Hits that fulfill the individual cuts don't have to fulfill the combined χ^2-cut when they lie at the edge of the cut. They can produce the peak with no time residual.
Besides the peak the spectra obtain the same shape independent of the tracking

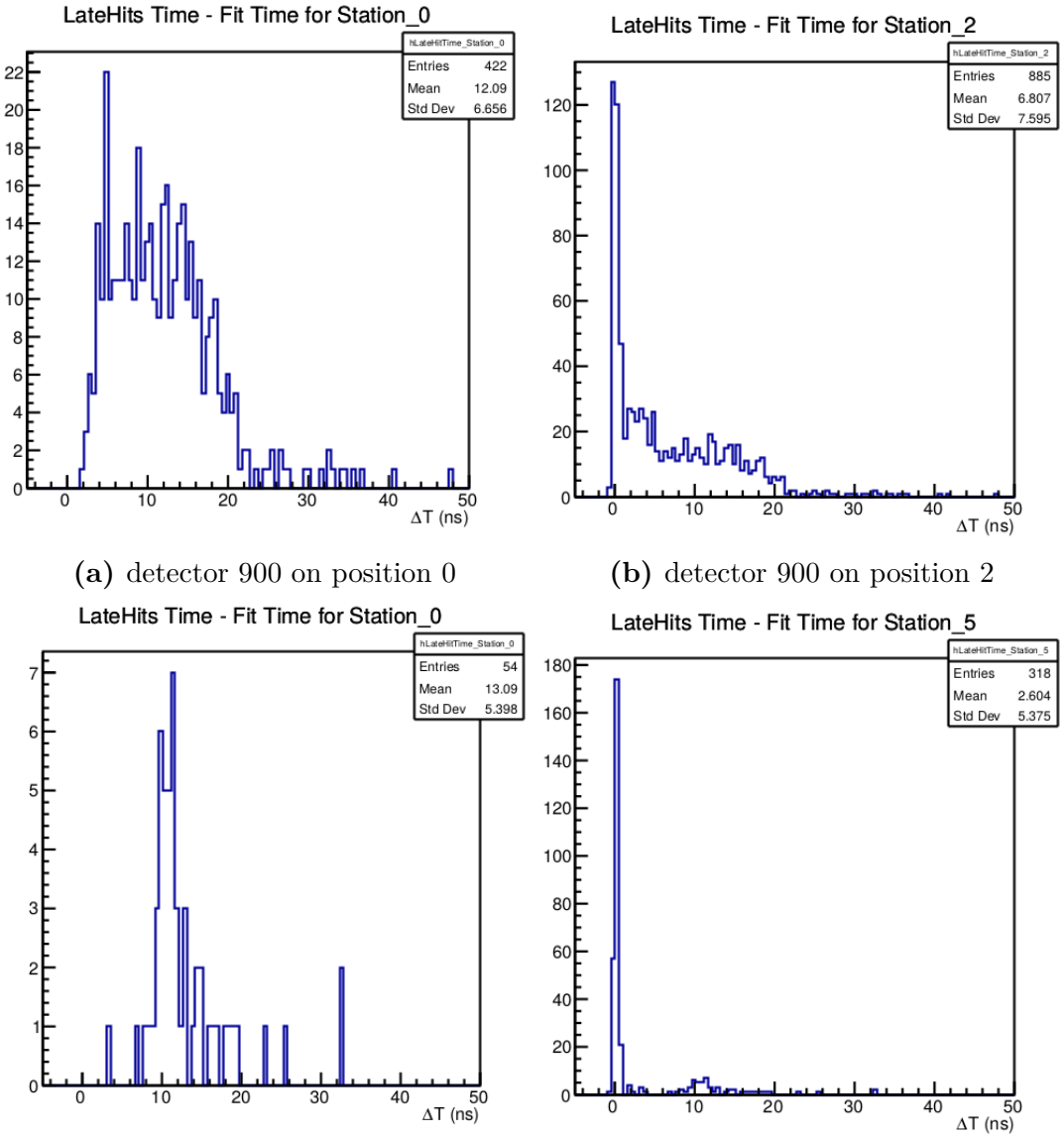

(a) detector 900 on position 0

(b) detector 900 on position 2

(c) detector 921 on position 0

(d) detector 921 on position 5

Figure 4.7: Time spectra of late hits for detector 900 and 921 on different positions in tracking setup. Both counter exhibit a clear late hit spectrum independent of the tracking setup. Only the peak at 0 differs which is due to cuts in the tracking algorithm.

position. This can be seen in 4.7a and 4.7b for detector 900 and in 4.7c and 4.7d for detector 921. These two detectors exhibited the strongest late hit spectrum. In total about 600 late Hits were found in 60000 events with tracks of

multiplicity 5 of run r0067. Detector 900 produced 422 of these, 921 contributed with 54. The other detectors almost have no late Hits. Combining several runs could improve the statistics of the spectra.
Further questions are whether the pronounced spectra appear because detector 900 and 921 are located on the top and bottom of the setup. One could also look for differences in the spectra between counters that aren't identical in construction, i.e. between 900 and 901 from THU and 911 to 921 from USTC. With the obtained statistics from one run, answers to these questions aren't meaningful.
The amount of late Hits would allow an estimation of efficiency measurements uncertainty. In previous measurements the after-pulse probability of the tested counters was determined[1]. It was found to be around 20%. The efficiencies of the detectors are measured to be around 95%. This means 5% probability of not measuring the first hit which then produces an after-pulse in 20% of the events. So a late hit should be present in 1% of the events which fits to the observed values of detector 900.
The explanation of a late hit is that the original hit in the detector was not picked up, but the after-pulse was detected. With the above calculation it is confirmed that the detectors have an efficiency of around 95%. For the final experiment it is desired to have efficiencies of 99% and higher since the theoretical limit of MRPCs lies above 99.9% efficiency.

[1] by Phillip Weidenkaff in his master thesis. not published

5 Summary and outlook

The ToF-wall of the future CBM experiment consists of MRPCs. Before that the detectors will be used in experiments like STAR or mCBM. These experiments start at the end of 2018 and are part of the FairPhase0 program. In order to test prototypes a cosmic test stand has been established in Heidelberg. For the measurements used in this thesis it consisted of six detectors that were arranged above each other. Incoming cosmic muons leave a track in the setup. These tracks can be reconstructed and fitted. Within CbmRoot exists analysis software that allows the determination of efficiency and time resolution of the tested detectors as well as other characteristics. At the working point of 112 kV/cm a time resolution of about 60 ps and an efficiency of about 95 % for all detectors was found.

An additional quality assurance tool is an event display. It can provide a 3D-model of the detector setup and a visual representation of an event. This allows debugging of reconstruction code for example as one can see the reaction of the tracker to specific instances.

To further improve the capabilities of the event display for the TOF test stand additional functionality was developed within the scope of this thesis.

It is now possible to represent the time of hits in a color coded fashion. The clustersize of hits is represented through the size of the markers. Also the time over threshold can be visualized. In order to change the appearance of the rendered points two GUI-components were programmed. The implementation of these features in the existing analysis chain in FairRoot required three new classes that were programmed in C++ and Root.

Other additional functionality that was developed includes a label that appears for every object and contains the relevant physical information of that object. For the hits this includes the time, ToT and clustersize. For fitted tracks and

corresponding points this label presents the velocity, goodness of fit and residuals in time and position.
Another part of this thesis was the study of possible applications for the event display. With the help of the additional functionality several events of the cosmic data were analyzed. The data was obtained in a run that took 22 h. This lead to about 600000 events.
Interest existed in the behavior of the tracker. It requires the specification of a tracking setup which defines the order in which the detectors are used in forming tracks. Reconstructed events are fitted with a straight line. Events were studied in which found tracks depended on the tracking setup. It was concluded that the commonly used tracking setup has a systematic weakness for reconstructing tracks that missed the top or bottom detector layer due to their angle. On the other hand this tracking setup is optimized for forming tracks that include hits in every detector layer. The amount of events where the "correct" tracks weren't found is estimated to be around 1 %. These effects become important when the efficiency is around 98 % and higher. Each tracking setup has some weaknesses to specific instances. One has to choose the setup according to the task one wants to perform and the detector characteristics one is interested in. For the upcoming mCBM experiment the current tracker will be replaced by a cellular automaton and Kalman-Filter tracker developed by groups within CBM[AK16].
A cosmic test stand with RPCs is commonly used to test the performance of these detectors. In order to quantify detector characteristics tracking of the muons is needed. Fitting a straight line is sufficient. The simplest approach is to fit a line to all points that are part of an event. One could define cuts like a maximum number of hits that are allowed per detector to sort out events with high noise. The tracker used in this thesis is much more sophisticated. It selects the right hits and doesn't use noise hits because they don't fit to the track for example. Another approach for a tracking algorithm with cosmic muons is being developed by D. Samuel and K. Suresh in India[SS18]. They developed an artificial neural network (ANN) based tracker. It fits straight lines to projections on the X/Z- and Y/Z-plane with image recognition. In contrast to their previous tracker based on a simple straight line fit this ANN-tracker is

more resilient to noise hits on the RPCs.
The event display was used to study events that contain clusters of sizes bigger than 10. The clustersize specifies the number of strips that contributed to one hit. The question was whether such clusters appear only once in an event or multiple times. The forming of clusters is done in a task called Clusterizer. It depends on a parameter called cluster-building-radius which defines how far away in Y and T a hit on the neighboring strip can be to still be merged in a cluster. In the analyzed data run 142 big clusters were found. The majority of events contained more than one big cluster. One example event was studied further. For this event the composition of one big cluster was studied by turning off the cluster-building-radius. It had a size of 17 contributing strips. In the event each detector layer had many hits that were all time correlated. This led to the conclusion that the event originated from a particle shower that was produced in the ceiling of the laboratory. The cluster therefore didn't originate from one particle but from many particles that came close in time and space and were merged to one cluster.
The last application that was studied was the search for late hits. A late hit is defined as a hit that fits in space to a reconstructed hit but was not merged to it due to a big time residual. The explanation for a late hit is that the original hit produced an after-pulse but was itself not detected. The obtained late hit spectra lack statistics to make quantified statements from them. This could be improved by analyzing more data runs. In previous studies the amount of after-pulses was obtained to be around 20 %. With an efficiency of 95 % this corresponds to 1 % of late hits in the relevant events. The search for late hits was done with tracks that missed only one detector layer. This occurred in about 60000 events. Around 600 late hits were found which fits the estimated 1 % for late hits.
In all the studied applications it was necessary to use the additional information provided by the event display to understand the event. This demonstrated that such an event display filled with physical information of the hits and tracks can be effectively used as an additional quality assurance tool. The event display was developed to also help with further studies that are interested in specific detector responses.

List of Figures

List of Tables

Bibliography

[Sha+06] Ming Shao et al. "Simulation study on the operation of a multi-gap resistive plate chamber". In: *Measurement Science and Technology* 17.1 (2006), p. 123. URL: http://stacks.iop.org/0957-0233/17/i=1/a=020.

[Ant+09] I. Antcheva et al. "ROOT: A C++ framework for petabyte data storage, statistical analysis and visualization". In: *Comput. Phys. Commun.* 180 (2009), pp. 2499–2512. DOI: 10.1016/j.cpc.2009.08.005. arXiv: 1508.07749 [physics.data-an].

[AK16] Valentina Akishina and Ivan Kisel. "4D Cellular Automaton Track Finder in the CBM Experiment". In: *EPJ Web Conf.* 127 (2016), p. 00003. DOI: 10.1051/epjconf/201612700003.

[DH18] I. Deppner and N. Herrmann. "The CBM Time-of-Flight system". In: *14th Workshop on Resistive Plate Chambers and Related Detectors (RCP2018) Puerto Vallarta, Jalisco State, Mexico, February 19-23, 2018*. 2018. arXiv: 1807.02070 [physics.ins-det].

[SS18] Deepak Samuel and Karthik Suresh. "Artificial Neural Networks-based Track Fitting of Cosmic Muons through Stacked Resistive Plate Chambers". In: (2018). arXiv: 1807.04625 [physics.ins-det].

[Tan+18] M. Tanabashi et al. "Review of Particle Physics". In: *Phys. Rev. D* 98 (3 Aug. 2018), p. 030001. DOI: 10.1103/PhysRevD.98.030001. URL: https://link.aps.org/doi/10.1103/PhysRevD.98.030001.

[TS18] *CBM Progress Report 2017*. Tech. rep. Darmstadt, 2018. DOI: 10.15120/GSI-2018-00485. URL: http://repository.gsi.de/record/209729.

[FAI] FAIR. *The stuff nuclear matter is made of*. URL: https://fair-center.eu/public/what-happens-at-fair/basic-science/nuclear-matter-physics.html.

[FP1] FP13. *Measurement of Muon Properties in the Advanced Students Laboratory*. Version 1.3. URL: https://www.physi.uni-heidelberg.de/Einrichtungen/FP/anleitungen/F13.pdf.

[Gui] ROOT - Reference Guide. *Event Display*. Version 6.15/01. URL: https://root.cern.ch/doc/master/group__TEve.html.

[RC] Bernice Rogowitz and Olivier Couet. *The Rainbow color map*. URL: https://root.cern.ch/rainbow-color-map.

Erklärung

Ich versichere, dass ich diese Arbeit selbstständig verfasst und keine anderen als die angegebenen Quellen und Hilfsmittel benutzt habe.

Heidelberg, den 28.09.2018,